2010

Maskless additive manufacturing of micro structures by laser sintering of nanoparticles

Vivekram Ramanathan

Recommended Citation

MASKLESS ADDITIVE MANUFACTURING OF MICRO STRUCTURES

BY LASER SINTERING OF NANOPARTICLES

by

VIVEKRAM RAMANATHAN

A THESIS

Presented to the Faculty of the Graduate School of the

MISSOURI UNIVERSITY OF SCIENCE AND TECHNOLOGY

In Partial Fulfillment of the Requirements for the Degree

MASTER OF SCIENCE IN MANUFACTURING ENGINEERING

2010

Approved by

Frank W. Liou, Advisor
Joseph W. Newkirk
Robert G. Landers

ABSTRACT

The focus of this study was to investigate an alternate microfabrication process of sintering nanoparticles using a patterned laser light to generate two dimensional (2D) and three dimensional (3D) geometries. With trends of producing electronic and medical devices using cheaper and faster technologies, a new procedure was developed to deposit and bond miniature patterns of silver nanoparticles onto silicon substrates.

The process consists of spraying silver nanoparticles onto the substrate while a patterned or modulated laser beam is focused onto the sprayed nanoparticles. These nanoparticles exposed under the modulated laser light undergo partial melting or sintering and adhere to the substrate. The substrate is then cleaned to remove the unexposed nanoparticles from the surface. The deposition thus obtained from the process yields a 2D micropattern. 3D parts are produced using a layer by layer manufacturing process in which a two dimensional pattern is deposited over another pattern repeatedly until the desired elevation is obtained.

The initial part of the thesis will discuss the experimental investigation on the influence of process parameter (i.e. flowrate, electric field distance, standoff distance and extractor size) on controlling the length, size and distribution of the spray to deposit nanoparticles. Later, the results of deposition and fabrication of microstructures using the process are presented.

ACKNOWLEDGMENTS

This research work is a result of some phenomenal help and support extended to me by numerous individuals at Missouri S&T. First of all, I would like to express my sincere gratitude towards my advisor Dr. Frank W. Liou for his guidance and support throughout my graduate program at Missouri S&T. Secondly, I would like to express my gratitude towards my committee members Dr. Jospeh W. Newkirk and Dr. Robert G. Landers for their advice and guidance during my graduate research. The research assistantship extended to me by Dr. Liou and the fellowship extended through the Manufacturing Engineering Program is deeply appreciated.

It has been a pleasure working with my colleagues at the Laser Aided Manufacturing Processes (LAMP) Laboratory. I would like to thank Todd Sparks and Jianzhong Ruan for their valuable inputs and suggestions which have been critical in completing my research. I would like to acknowledge Gurpratap for assisting me in taking SEM images, Eric Bohannan for help extended in obtaining AFM images, Shyam for assisting me with image analysis, John for helping me with the electrical circuitry and my colleagues at LAMP laboratory for their help and support. I would also like to acknowledge the Missouri S&T Mechanical Engineering Technical Shop staff especially Bob Hribar and Joe Boze for constructing the various experimental setups and Mitch Cottrell for assisting with troubleshooting the equipment used.

Finally, I would like to thank my family for their love, continued support and encouragement throughout my academic career.

TABLE OF CONTENTS

LIST OF ILLUSTRATIONS

LIST OF TABLES

NOMENCLATURE

Symbol	Description
V_{im}	Impact velocity
V_{cr}	Critical velocity
k	Boltzmann constant
T	Temperature
ρ_p	Nanoparticle density
D_p	Nanoparticle diameter
V_{cr}	Critical velocity
A	Hamaker constant
Z	Seperation distance
$K_{s.p}$	Mechanical constants of surface and particle respectively
$\sigma_{s,p}$	Specific adhesion energy of surface and particle respectively
υ_o	Flowrate
I	Current
a	Proportionality constant
K	Conductivity
σ	Surface tension
D_d	Droplet diameter
C	Proportionality constant
ρ_s	Solution density
ε_0	Dielectric constant of vacuum

q	Charge on droplet
μ	Viscosity of medium
E	Electric field
V_d	Droplet velocity
V	Electric potential
s	Standoff distance
$\varphi_{a,c}$	Diameter of anode and cathode ring respectively
$\Delta_{a,c}$	Displacement from reference plane of anode and cathode respectively

1. INTRODUCTION

1.1. PREFACE

Over the past decade, the need for rapid production of micro and nano sized components has expanded vastly due to development of new technologies. Commercially available products such as MEMS devices and Integrated Circuits (IC's) have proven the advantage and need of integrating miniature sensors and actuators to a variety of newer products. Increasing demand for smaller and powerful portable devices for applications from personal products such as iPod's to modern day sophisticated military equipment that require high computing power has inflated the need to develop advanced manufacturing processes and techniques to achieve quicker and cheaper fabrication of micro components. Thus, the need for newer manufacturing processes is of special interest and research.

Microfabrication and nanofabrication has traditionally been used for manufacturing semiconductors and IC components. However, blending multidisciplinary sciences such as medicine, engineering, material science, chemistry and biology has enlarged the need for micro fabricated products for newer applications like biotechnology (micro chemical reactors), energy (solar cells, fuel cells, portable batteries), medical (in vitro diagnostics, lab on chip) and numerous other potential applications.

Conventional subtractive processes such as micromachining (turning, milling, grinding), chemical processes (micro EDM, micro ECM) and ablation processes (laser, e-beam, focused ion beam) have been successful in manufacturing micro and nano devices. However these downscaled processes suffer from the fact that producing even a simple part could require a series of operations usually using different machines which results in

increased production cost per part. Alternatively, the use of traditional micro-fabrication techniques such as CVD, PVD and lithography require expensive facilities, long turnaround times and extreme process conditions.

New developments in fabrication technology have enabled fabrication of micro and nano structures in single and multiple steps. It reduces the cost of production but would be too slow to be used in a mass production environment. These techniques such as direct writing (e.g. SLS, inkjet, dip coating), micro-contact and offset liquid embossing allow for a more flexible 2D and 3D fabrication without the need for expensive tooling, equipment and sacrificial masks.

1.2. BACKGROUND

The following study is a continuation of a new direct micro-fabrication process developed at the Laser Aided Manufacturing Processes Laboratory at Missouri University of Science and Technology (Missouri S&T) [1]. Two dimensional layers are deposited onto a silicon substrate by combining a mask less laser pattern (obtained using a dynamic light modulation unit) with a coaxial nanoparticle flow generated using an aerosol generator. The nanoparticles are deposited onto the substrate by focusing them using a coaxial nozzle and the desired pattern is sintered onto the substrate by exposing deposited nanoparticles to a modulated laser beam. The final deposition structure is obtained by rinsing the substrate in a suitable solvent, such as ethanol or distilled water, where the unexposed nanoparticles are washed away leaving the sintered pattern affixed on the substrate.

The apparatus consists of a system to transport nanoparticles and another to generate the laser pattern used to sinter a 2D layer. Fine plume consisting of nanoparticles is obtained from an electrospray aerosol generator, a device used to atomize a solution into very fine droplets by the principle of electrospraying or electro hydrodynamic spraying. Silver nanoparticles were mixed in ethanol to obtain a homogeneous solution free from agglomerated nanoparticles as the nanoparticle ink.

When a high voltage is supplied to the electrospray aerosol generator, electrical shear stress elongates the liquid meniscus at the capillary tip which disintegrates into a spray of fine droplets. The ethanol in the ink solution evaporates leaving behind a fine plume of nanoparticles that are carried using nitrogen to the coaxial nozzle. The coaxial nozzle is used to collimate and accelerate the nanoparticles onto the substrate. During collision, the nanoparticles either temporarily adhere to the substrate surface or rebound on collision with the surface. Temporary adhesion of nanoparticles occurs due to the loss of kinetic energy of the particles and is kept in place by surface tension. To ensure complete bonding of the nanoparticles in the required shape, the laser pattern is applied to partially melt and bond the particles together.

The laser pattern is generated using a micromirror array commercially known as a Digital Micromirror Device (DMD). The generated pattern is focused using a long-working distance objective lens onto the silicon wafer that is placed past the focal point. The laser pattern is focused down to a micro scale on the substrate. The pre located film of nanoparticles is exposed to the generated 2D laser pattern to selectively sinter the nanoparticles and produce a continuous thin layer of the microstructure. The substrate is washed to remove the loosely bonded nanoparticles from the deposit leaving the bonded

pattern behind. By continuously spraying nanoparticles and exposing them to the generated laser pattern, the thickness of the microstructure is increased. 3D microstructures are produced by depositing one layer over an existing layer, a layer by layer fabrication technique.

1.3. GOALS AND LIMITATIONS

From preceding work [1] it is known that the process of depositing and sintering nanoparticles had a few major drawbacks. In relation to the concentration of the nanoparticle ink solution, only a small percentage of nanoparticles were transported to the substrate whereas a majority of the nanoparticles were accumulated at the tubing of the nanoparticle flow. The depositions obtained had a low coverage area, i.e. a low packing density of nanoparticles over an area and thus the structure deposited was found to have voids in deposition and incomplete conductive paths. Thus, the microstructures obtained were ineffective to be used as an electrical circuit. This inefficiency to deposit a well distributed area of nanoparticles was contributed to the fact that an effective nanoparticle collimation system was not in effect during the deposition process.

Thus, the current work was focused towards identifying an effective mechanism to transport, collimate and improve the coverage of nanoparticles over an area. By doing so, the expected outcome was a small sized deposition consisting of thin layers of sintered nanoparticles having an even surface without massive agglomerations and voids. Furthermore, consideration was given to develop an effective system that would provide repeatable depositions while making the apparatus cost effective, compact and portable.

2. LITERATURE REVIEW

2.1. DIRECT WRITE LITHOGRAPHY

The shortcoming of traditional lithography has been overcome by new direct write processes. The need to develop a photoresist over a metal part to protect the surface during etching is labor intensive, time consuming and expensive when compared to depositing the required pattern over the substrate directly in a single step.

A variety of direct write based systems [1-10] have been developed for fabricating microstructures. Most of these systems share a common feature of using a laser beam to sinter nanoparticles onto the substrate but their primary difference lies in their mechanism of depositing nanoparticles onto the substrate. Bieri et al. [2-4] use a drop on demand system to place nanoparticle ink droplets onto a substrate following which a laser beam was used to evaporate the solvent and sinter the nanoparticles. The drop on demand ink system uses piezoelectric pulsed vibrations to generate microdroplets from a glass tube. A similar system using a micropipette working similar to a fountain pen was developed by Choi and Pouloikakos [9].

Ko et al. [7] have deposited gold nanoparticles onto a temperature sensitive polymer substrate by utilizing an inkjet print system. In the process, nanoparticles in the form of ink was printed onto a substrate, dried and sintered using a continuous laser beam. Sintering of wet nanoparticles cause rim like formations [4] due to displacement of nanoparticles around the heated region of the laser beam. Fuller et al. [8] built MEMS and micro electric circuitry by maintaining the substrate at elevated temperatures using a hotplate to flash evaporate the nanoparticles ink possibly avoiding the rim formation caused by localized heating of wet nanoparticle ink. When the substrate was maintained

at high temperatures, droplets dried rapidly leaving behind an uneven surface of continuous dots. While the substrate was maintained at lower temperatures, the slower evaporation created a continuous line having a uniform cross section.

In the above mentioned literatures, the processes make use of pre-locating nanoparticles onto the substrate before they are cured or sintered to form the microstructure. These processes operate in parallel, i.e. the nanoparticles are placed at one point while curing or sintering occurs at another point during the process. Nadgorny et al. [5, 6] have developed a system to continuously deposit and bond nanoparticles at the same time using laser induced optical forces to transport nanoparticles onto the substrate. The dynamics of the nanoparticles are controlled by optical transverse gradient forces to confine particles inside a weakly focused laser beam and move them towards the substrate.

Another technique of direct writing nanoparticles was applied by Lee et al. [10] to pattern micro electrical inductors by using a nano-colloid jet. The jet was obtained by electrospraying a solution containing nanoparticles suspended in ethylene glycol and surfactants in the cone jet mode. The advantage of this process over the ink jet or drop on demand technology is the ability to use a variety of nanoparticle ink solutions. While high viscosity solutions are highly unfavorable in ink jet and drop on demand, they can be easily deposited using the electrospraying technique. Moreover, an electrospray produces a continuous flow and placement of nanoparticles unlike the rapidly pulsed flow of ink jetting.

2.2. MASKLESS FABRICATION

Traditional microfabrication processes make use of a photo mask to selectively expose and generate photo polymerized patterns. The multiple steps applied to generate the masks, render the process to be time consuming, expensive and cumbersome. These drawbacks have been overcome by implementing a dynamic mask, typically using a Liquid Crystal Display (LCD) or a Digital Micromirror Device (DMD). Several new direct write processes [11-16] based on sintering and photopolymer curing have been developed by using dynamic masks.

Sun et al. [11] have demonstrated the use of a high resolution projection micro stereolithography process using a dynamic mask to fabricate complex three dimensional structures by UV curing of resin. Similar microstereolithography systems [12-16] have been developed to fabricate microstructures that take advantage of using a dynamic mask to cure a layer rather than raster scanning. In a vector-by-vector processing approach, layers are formed by raster scanning over an area. However, in the integral approach, a complete layer is cured due to irradiation of the complete layer. This process has been efficient in producing parts of generally smaller sizes in the range of a few hundred microns or less. In most stereolithography curing processes, the cured portion of the resin is immersed into the liquid resin to provide another layer for sequential exposure or the liquid resin is spread over the cured area using a blade. Thus these processes are intermittent between resin layering and pattern exposure.

Developments have shown that the use of LCD as a dynamic mask has limited optical efficiency compared to a Digital Micromirror Device (DMD, Texas Instruments). The difference in performance between the two has been tabulated by Sun et al. [11] and

some important shortcomings of using a LCD as a dynamic mask are lower modulation efficiency, pixel size filling ratio and switching speed.

Vertical resolution of the obtained part is determined by the individual thickness of layers. Smaller layer thickness produces better resolution but requires an increased number of layers to build the part. Lateral resolution of the obtained components is decided by the size and number of individual micromirrors and the focusing lens system. The resolution of the masking layer can be improved using multiple micromirrors as shown by Zhou [16] and Chen. When multiple micromirrors are used to project a beam with a slight overlap between them, the size of the individual pixels can be reduced. The light intensity of every micromirror is maintained lower than the required critical intensity. During overlapping, the overlapping pixel area is subjected to intensity above the critical intensity due to which curing or sintering occurs.

Xu et al. [14] studied the uniformity in distribution of the reflected light intensity from a micromirror array. The distribution of the reflected light intensity was found to be uneven and thus prototyping imprecise micro parts. It is proposed that by controlling the grayscale of the individual micromirrors, superior uniform distribution of light intensity can be obtained.

2.3. FLOW AND TRANSPORTATION OF NANOPARTICLES

2.3.1. Nanoparticle Atomization. Dispersed aerosols are commonly generated from solutions by nebulization, a process in which gas is passed through a liquid solution to generate a fine atomized spray. Monodisperse and well atomized sprays have been obtained by subjecting a solution to a high potential in a process known as "Electrospray

Ionization". This process is generally referred to as "Electrospraying" or "Electrohydrodynamic Atomization (EHDA)". It is an effective method to generate charged aerosols [17] when compared to nebulization since the atomized droplets produced are of smaller size and smaller charge. The flow of the droplets or particles can be controlled to a limited extent by adjusting the input flowrate and applied voltage. Sir Geoffrey Taylor [B3] pioneered the basics of electrospraying theory. The theory was later improved by others [20, 25–30].

Liquid passing through a capillary tube is subjected to a high potential. At the tip, i.e. end of the capillary, the liquid meniscus is subjected to an electric field which is counteracted by surface tension. With increasing electric potential, the field generated becomes stronger and after a limit prevails over surface tension. The liquid present in the capillary tip or the emitter is elongated due to the shear stress caused by the electric forces on the surface of the liquid. The liquid meniscus later deforms into a fine mist of droplets (or plume) due to instability caused by excessive charging as the liquid shrinks due to evaporation. Nanoparticles are transported using a liquid solution as a transportation medium which in due course evaporates completely, generating a finely distributed spray of nanoparticles.

The type of spray obtained from the process varies with applied voltage, rate of liquid flow and the physical properties of the liquid used. The types of spray obtained have been studied [21– 23] and are classified by the geometric form of the liquid at the emitter outlet and the mechanism of droplet disintegration. The spraying mode of crucial interest in most practical applications [17, 18] has been the cone jet mode.

In the cone jet mode, it was found that the liquid meniscus at the emitter tip forms a cone shape (linear, concave or convex) which extends to a thin jet that flows along the axis [24]. The cone and the jet formed are stable, i.e. the cone formed is axisymmetric and is limited to slight or no physical movement. The disintegration of the spray in this mode produces droplets of uniform size and the theory behind the jet break up was given by Hartman et al. [24]. For lower flowrates, typically in the range of µl/min and nl/min, slight different spraying characteristics were observed. The low flowrate generates smaller initial droplets and the spraying has been classified as "Microspray" or "Nanospray".

To obtain better spray deposition morphology, Rietvelt et al. [26] have developed a model to study various electrospray deposition parameters. The deposition process was classified into four processes (cone stability, jet breakup, evaporation and deposition) to examine the various factors influencing the spray. His findings suggest that, with increasing distance between the emitter and the substrate, the radius of spray increases. Also, when the distance between the emitter and substrate is small, most of the nanoparticles are washed away due to wetness and as the distance was increased, the deposition began to form agglomerates and finally thin films. A trend of increased deposition surface roughness was observed with increasing standoff distance.

It has been reported that voltage has minimal effects on the obtained spray. A study by Smith et al. [27, 28] suggests that the voltage applied to an electrospray was found to be linear with changing flowrate. The sensitivity of the voltage was found to be influenced by the resistance of the flow system and emitter outer diameter.

2.3.2. Aerodynamic Lenses. Nanoparticles have been a challenge to focus due to their inherent properties of low inertia and high diffusivity. Due to their low inertia, the nanoparticles tend to follow the streamlines of the carrier gas and their high diffusivity tends to broaden the beam of particles. Early experiments to achieve collimated beams and reduce particle divergence were achieved using sheath gas have been successful. But, aerodynamic lenses [31-36] have been used to produce tightly collimated beams of nanoparticles making use of their low inertia by alternately compressing and expanding the carrier gas.

As proposed by Wang et al. [31, 32], the deviation of nanoparticles from their trajectory is determined by the particles Stokes number. The flow through the orifice is required to be continuum, subsonic and laminar (Re < 120). The optimum Stokes number for axial trajectory flow was found to be 1. To achieve Stokes number of 1, very low pressure or small orifices in the lens are proposed. However, operating at very low pressure enhances the effects of diffusion whereas using small orifices limit flowrate, clog and result in increased Reynolds number. Since Stokes number is a function of the material density, an aerodynamic lens system could be ineffective to focus different particle beams.

Wang et al. [32] assume that the aerodynamic lenses are responsible for all focusing and the particles are assumed to be spherical and neutrally charged. Reynolds number above which flow instability and turbulence disperse particles causing defocused beams is not clear, thus the Reynolds number used is assumed to be below 200.

In another study by Lee et al. [34], it was found that the parameters Reynolds number, Mach number and upstream pressure are interrelated and affected by the

geometry of the lens and system factors. Thus, the parameters are not to be treated as independent variables as in the earlier studies by Wang et al.

2.3.3. Surface Collision of Nanoparticles. Collision of nanoparticles with a substrate or filtration medium has been studied theoretically, experimentally and verified using simulations [37-40]. It is found that the adhesion of nanoparticles to a substrate depends on the loss of center-of-mass energy of the particles due to collision. The energy loss mechanism is not clearly understood as yet. While some studies have attributed the energy loss to plastic deformation of the particles or the substrate, other studies have attributed the mechanism of energy loss to be dissipated in heat forms during collision.

Wang [38] and Kasper proposed that the adhesion efficiency of nanoparticles is defined by two parameters, impact velocity and critical velocity, and derived the equation for the two. The impact velocity [V_{im}] is assumed to follow a Maxwell-Boltzmann distribution and is given by,

$$V_{im} = \sqrt{\frac{48kT}{\pi^2 \rho_p D_p^3}}$$

(2.1)

where k denotes the Boltzmann constant, T denotes the temperature and ρ_p, D_p denotes the particle density and diameter respectively.

Critical velocity [Vcr], defined as the maximum impact velocity above which rebound occurs is given by two models, B-H theory (Bradley-Hamaker) and JKR (Johnson-Kendall-Roberts) theory. The critical velocity given by the BH model is,

$$V_{cr} = \sqrt{\frac{A}{\pi \rho_p Z D_p^2}}$$

(2.2)

where A is the Hamaker constant, Z is the minimum separation distance and ρ_p, D_p are the particle density and diameter respectively. The critical velocity based on the JKR model is given by

$$V_{cr} = \left[\frac{3^7 \pi^4 (K_s + K_p)^2 \sigma_{p,s}^5}{\rho_p^3 D_p^5} \right]^{1/6}$$

(2.3)

where $K_{p,s}$ are mechanical constants (obtained using Young's modulus and Poisson ratio with respect to the material) of the particle and surface respectively, $\sigma_{p,s}$ is the specific adhesion energy of the particle and surface respectively and ρ_p, D_p are the particle density and diameter respectively.

From both the theories, BH and JKR, it is apparent that the critical velocity decreases with increasing particle diameter. In a molecular dynamics simulation study using silver nanoparticles [39], the study suggests that thermal rebound was possible at elevated temperatures. There is also the possibility of weakly bonded nanoparticles leaving the surface.

2.4. CHARACTERISITCS OF SILVER NANOPARTICLES

2.4.1 Properties of Silver Nanoparticles. Nanoparticles exhibit different mechanical, chemical, optical and electrical properties that are not observed in their bulk counterparts due to the large surface to volume ratio, large surface energy and spatial confinement. High surface to volume ratio for nanoparticles have been used to improve the performance of catalysts. Silver has primarily been used as the base element for micro-component electrical conductivity for its excellent electrical properties. Although copper is relatively inexpensive compared to silver, the formation of copper oxides has

proved to be challenging for manufacturing micro-scale electrical devices. The intrinsic conductive properties of individual particles are high, however when they agglomerate, the contact resistance can become high as well. It was demonstrated that silver nanoparticles on being sintered exhibited greater resistance compared to bulk silver by about 5 times [10].

The primary advantage of using nanoparticles for fabrication is due to their remarkably lower melting temperatures compared to bulk materials [41-48]. Due to the phenomenon of melting point depression whereby when the particle size decreases, nanoparticles have a larger surface to volume ratio which alters their thermodynamic parameters. Thus nanoparticles in general are bonded at much lower temperatures compared to bulk materials and hence can be easily sintered onto a wide range of substrates including polymers, plastics and temperature sensitive substances.

The melting point for gold nanoparticles in the range of a few nanometers was found to be approximately 300 to 400°C versus 1064 °C for bulk gold [44]. It was found that nanoparticles having diameters less than about 50nm had a sharp decrease in melting temperature [45]. In an investigation [48] on the sintering behavior of 20nm silver nanoparticles, the nanoparticles exhibited sintering behavior at significantly lower temperatures of 150°C compared to 960°C bulk melting temperature of silver. The results also showed that with increasing annealing temperature, the size of the coalesced particles and the crystallite size of the particles increased. The electrical conductivity increased almost linearly with increasing sintering temperature

Optically, nanoparticles change color due to quantum size effects. This is explained by Mie Theory where light-scattering by a sphere is described. Nanoparticles

can be manipulated by using very small forces using a focused laser beam. Strong electric field gradients are found at the waist of the beam (depth of focus) and the particles are attracted to the strongest electric field. These forces also tend to propagate nanoparticles towards the direction of the laser beam.

2.4.2. Safety and Toxicology. Although silver nanoparticles are used for commercial applications such as cosmetics, food packaging, therapeutics and antimicrobial applications extensively, their effects to the human body and their effects on the environment on waste disposal have minimal understanding. The lack of in-depth study poses a threat to the human body and the environment.

According to a study by Valiyaveetil et al. [49], their findings on the effects of silver nanoparticles on zebrafish describe the ill effects of silver nanoparticles on zebrafish embryos. Embryos exposed to silver nanoparticles were found to have nanoparticles deposited in vital organs resulting in phenotypic defects, altered physiological functions and degenerated body parts. Exposure to silver nanoparticles resulted in accumulation of blood causing necrosis. According to another study by Jin-Sook Hyun et al. [50], prolonged exposure of silver nanoparticles in rats indicate that silver nanoparticles have an influence on the respiratory system but without toxicological significance. In humans however, prolonged exposure to silver nanoparticles is known to cause "Argyria" a condition in which skin is decolorized to a blue or bluish-grey color. Generally, silver is believed to exhibit low toxicity in the human body and its effects are believed not to be life threatening. However, since silver nanoparticles are small enough to be inhaled and could also possibly penetrate human skin it is still a concern.

3. ELECTROSPRAY ATOMIZATION THEORY

Electrospraying (electrohydrodynamic spraying) is a technique used to disperse a liquid into a fine aerosol of liquid droplets (atomization) through electrostatic charging rather than employing pneumatic methods such as nebulization. The plume of droplets is generated by electrically charging the liquid to a very high voltage. Electrospraying has the following advantages over conventional atomization techniques:

- Droplets of smaller size are produced

- Size distribution of droplets is narrow having small standard deviation

- Droplets are self-dispersing due to mutual repulsion of charges resulting in the absence of droplet coagulation

- Motion of the charged droplets can be controlled using electric fields

- Deposition efficiency of charged droplets is higher than un-charged droplets

An electric field is applied between the nozzle and a counter electrode for a liquid flowing through a capillary. This electric field induces a surface charge in the growing droplet at the nozzle. The surface charge and the electric field create an electric stress at the liquid surface. The charged liquid meniscus in the nozzle becomes unstable as it is forced to hold more and more charge. Once the liquid reaches a critical point at which it can no longer hold an electrical charge, the liquid meniscus at the tip of the nozzle blows apart into a cloud of tiny, highly charged droplets. These charged droplets fly about seeking a potential surface opposite in charge to land on. During their flight, these droplets rapidly shrink as solvent molecules evaporate from their surface. Due to their shrinking size, the distance between electrical charges in the droplet dramatically

decreases. As these droplets seek a deposition surface to dissipate the charge, the electrical charge within the droplet reaches a critical state where it cannot hold charge any longer and violently blows up again. The droplet continually shrinks until it either dissipates its charge onto a surface or undergoes complete evaporation leaving behind a finely dispersed plume of particles. The breakup progression of a charged droplet is depicted in Figure 3.1.

Charged droplet undergoing evaporation

Droplets repeatedly breakup into smaller droplets due to charging and undergo evaporation

Finally obtained plume of nanoparticles
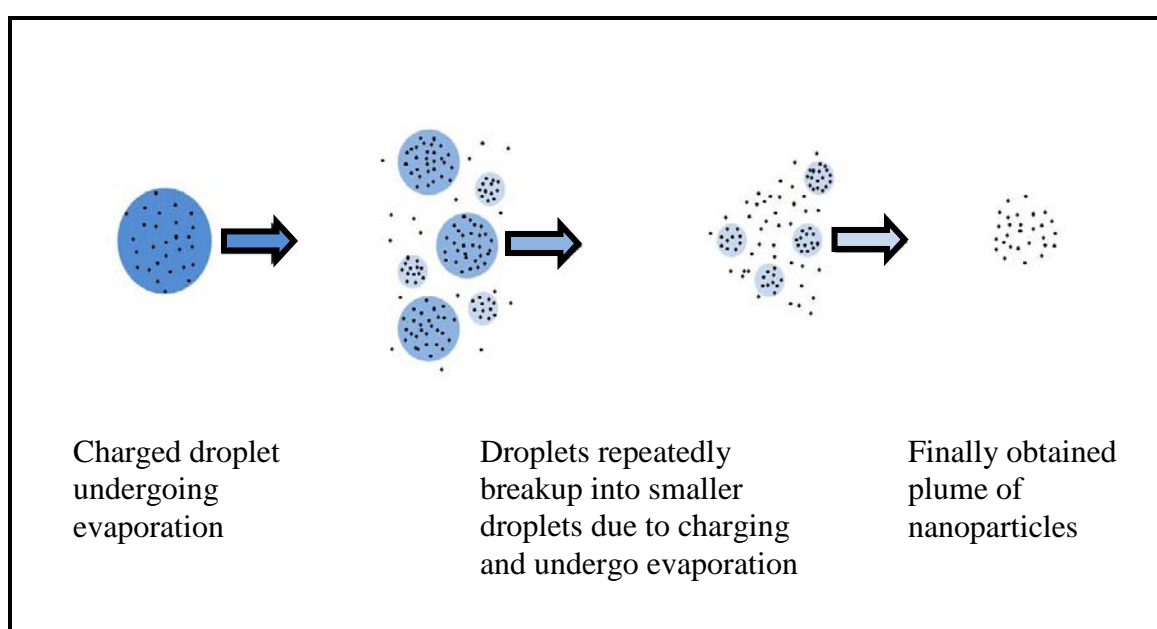
Figure 3.1 Breakup progression of charged droplet after electrospraying

Depending on the strength of the electric stresses induced in the liquid surface relative to the surface tension stresses, the liquid meniscus undergoes deformation and the liquid is emitted from the nozzle due to kinetic energy. Different spraying modes are obtained depending upon the deformation of the meniscus and the kinetic energy of droplet disintegration which is determined by the applied voltage. During lower voltages, the instability in flow causes a drop like disintegration. At larger voltages, a random

chaotic disintegration is found. At point in between, for an appropriate voltage, a stationary axis symmetrical stable cone and jet are obtained. The modes of electrospraying are distinguished in literature [20 - 23] depending upon the formation of the meniscus, motion of the jet and the disintegration of the liquid into droplets. These modes can be classified into two principal categories, each having different modes of operation:

- Dripping modes: fragments of liquid droplets are directly ejected from the capillary nozzle. These liquid fragments can be ejected as regular large droplets (dripping mode), fine droplets (microdripping mode), elongated spindles (spindle or multispindle modes) and sometimes irregular fragments of liquid

- Jet modes: the liquid elongates into a long, fine jet before being ejected from the capillary nozzle. The fine long jet can be smooth and stable (cone-jet mode) or regularly rotate around the capillary axis (precession mode) or oscillate in its plane (oscillating mode) or as a few fine jets on the circumference of the capillary (multiple-jet mode). The jet disintegrates into droplets due to electrostatic forces

The most important mode of spraying is the cone-jet mode. In this mode, the liquid meniscus assumes the form of regular, axisymmetric cone with a thin jet at its apex, stretching along the capillary axis. The stable spray said to be operating in the cone jet mode is shown in Figure 3.2. According to Hartman et al. [24], the size distribution produced by electrospraying in the cone-jet mode depends on the diameter of the jet and

its breakup into droplets. The jet break-up occurs due to two types of instabilities, varicose or kink. In the case of varicose instabilities, the jet disintegrates into equal droplets which flow along the capillary axis. In the case of kink instabilities, the end of the jet moves irregularly and breaks up into series of droplets, possibly due to the inertial and repulsive electric forces.
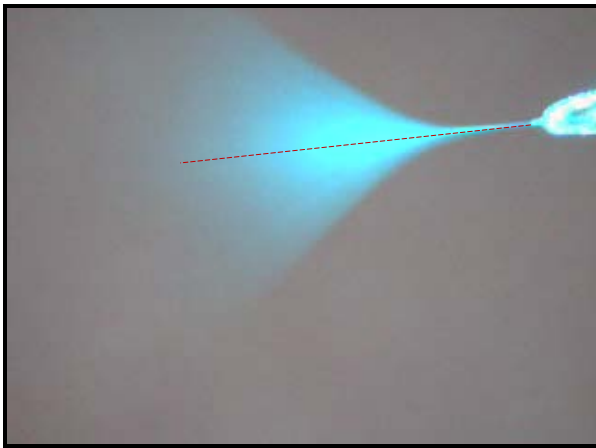

Figure 3.2 Liquid sprayed in cone jet mode. The stable axis symmetric spray was achieved by supplying high voltage between shown capillary and cathode

At a minimum flow rate, the jet breaks up due to axisymmetric instabilities called varicose instabilities and at higher flow rates, the current through the liquid cone increases. With increasing current the surface charge on the jet increases and above a certain surface charge, the jet break-up is also influenced by lateral instabilities of the jet called kink instabilities. When the influence of these kink instabilities increases, the size distribution of the primary droplets becomes wider.

To estimate the right conditions and process parameters, scaling laws have been developed to estimate the jet diameter and the electric current during extraction of liquid in a cone jet mode. Hartman et al. [24] theoretically derived the relations for

electrospraying processes as a function of the flowrate and liquid properties. The relation for current (I) for a flat velocity profile is given by

$$I = a \, (K \upsilon_0 \sigma)^{1/2} \tag{3.1}$$

where a is the proportionality constant, K is the conductivity of the liquid, υ_0 is the flowrate and σ is the surface tension. The droplet diameter in a jet breakup is determined by the ratio of electric stresses and surface tension. For lower electric stresses, the droplet diameter (D_d) for a varicose instability is given by

$$D_d = C \, (\rho_s \mathcal{E}_0 \upsilon_0^4 / I^2)^{1/6} \tag{3.2}$$

but when the ratio between electric stresses and surface tension exceeds 0.3, the jet breakup occurs due to kink instabilities and the droplet size is derived from the Reyleigh limit and the droplet size (D_d) is given by [26]

$$D_d = (0.8 * 2.88 \mathcal{E}_0 \sigma \upsilon_0^2 / I^2)^{1/3} \tag{3.3}$$

where C is the proportionality constant, ρ_s is the density of the solution, $\mathcal{E}_0$ is the dielectric constant of vacuum, υ_0 is the flowrate, σ is the surface tension and I, the current in the droplet. As the droplet evaporates, the charge in the droplet does not alter until the Rayleigh limit is reached. Assuming the charge to be evenly distributed over the droplets, the maximum charge on a droplet is defined [26] as

$$q_{max} = \pi (8 \mathcal{E}_0 \sigma D_d^3)^{1/2} \tag{3.4}$$

where $\mathcal{E}_0$ is the dielectric constant of vacuum, σ is the surface tension and D_d is the calculated diameter of the droplet. The electric field can be approximated when the extractor (cathode ring) is around the tip of the emitter. Assuming a constant potential, the field can be expressed [26] as

$$E = \Delta V / s \tag{3.5}$$

where ΔV is the difference in potential between the extractor-emitter and the substrate; and s is the distance between the emitter and the substrate. Droplets are ejected with an initial velocity from the jet. The initial droplet velocity can be obtained assuming that the flowrate of the spray is conserved in the jet and neglecting the interaction between charged particles. However, since the droplet is quickly dominated by the balance of drag forces and viscous drag forces, a simplified equation for droplet velocity is given by

$$V_d = Eq/3\pi\mu D_d \tag{3.6}$$

where E is the electric field, q is the charge on the droplet, μ is the viscosity of the medium (air) and D_d is the diameter of the droplet. Rietveld et al. [26] also experimentally derived a relationship between the standoff distance (from a stationary nozzle to a substrate) and the radius of the nanoparticle film deposition. For standoff distances between 1 and 7 cm, the relation for the radius of film formed (R_{film}) is given by,

$$R_{film} = (4.7 \pm 0.2)s^2 + (0.16 \pm 0.01)s \tag{3.7}$$

where s is the distance between a stationary nozzle and the substrate. However, the relationship holds good only for the parameters used in the experiment. The equation would vary depending on the current (higher current would increase repulsion between droplets creating a larger film radius), solvent (due to their charge density, conductivity, viscosity) and spray geometry.

4. DEPOSITION PARAMETER INVESTIGATIONS

In order to develop an effective nanoparticles transportation and deposition system, formation of the spray cone and characteristics of nanoparticle depositions using an electrospray were investigated. Since nanoparticles are highly diffusive, the absence of a carrier gas was apparent to improve the deposition of nanoparticles onto a substrate. Furthermore, the possibility of generating a fine plume of nanoparticles just ahead of the substrate was anticipated to produce a narrower and denser desposition of nanoparticles on the substrate. The parameters that influence the electrospray and their place of origin are listed in Table 4.1.

Table 4.1 Parameters that influence an electrospray and their origin [26]

Origin	*Influencing Parameters of Electrospray*
Setup	Flow rate, Growth rate, Temperature, Spray geometry, Electric field, Emitter geometry
Solute	Surface tension, Vapor pressure, Relative permittivity, Density, Viscosity, Conductivity, Solubility
Solvent	Concentration, Density, Viscosity, Conductivity
Substrate	Surface structure

The proposed investigation setup consists of a capillary needle (the tip of the capillary also referred to as "Emitter") through which an ethanol (unless otherwise stated) ink solution is flowed. The emitter is supplied with a high positive voltage while a cathode ring (also referred to as "Extractor") is connected to the negative and is placed facing the emitter. A monochromatic laser light is passed through a beam expander

(Edmund optics, 5X) to enlarge the laser beam. The expanded laser beam is used to illuminate the spray profile. A CCD camera microscope placed directly above the emitter was used to monitor and image the spray profile. Figure 4.1 illustrates the general experimental setup used to the study the deposition parameters. Additional equipment was used to ease facilitating individual experiments.
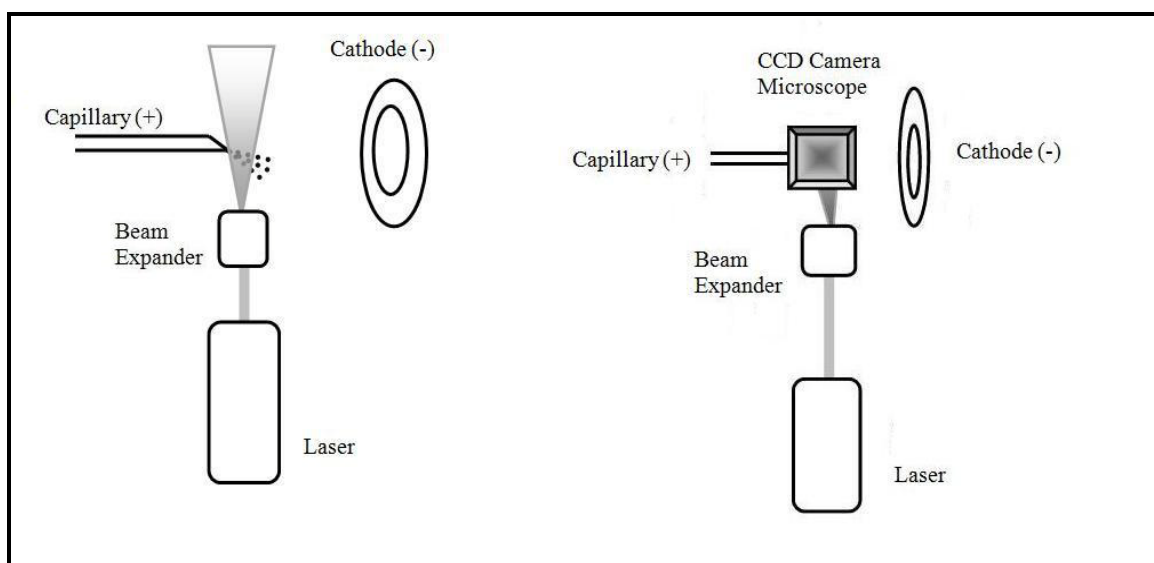

Figure 4.1 Setup arrangements for investigating deposition parameters. Note divergence of laser beam passing through spray. Shown is the apparatus setup viewed from front (left) and top (right)

The images obtained were analyzed to identify the influence of those parameters. These investigations were primarily focused towards identifying suitable parameters that could be used to attain a narrower spray having greater concentration of nanoparticles around the central axis of spray. The spray was analyzed for changes in the length of jet obtained, shape of spray and the illumination intensity, i.e. the brightness of the laser beam across the spray profile.

4.1. INVESTIGATION OF EMITTER SHAPE

During experiments, a difference in direction of the electrospray generated was observed. In theory, while electrospraying in the cone jet mode, the spray forms a jet having its axis along the axis of the emitter. However, the spray obtained during experiments was offset by an angle, the angle being approximately equal to the slant angle of the capillary needle tip. The probable cause of the irregular spray was attributed to the cross sectional profile of the emitter geometry. The experiment was used to study the causes of the irregular spray direction.

The experimental setup used to study the spray is shown in Figure 4.1. A low viscosity fluid solution; ethanol was flowed through the capillary emitter having a prefabricated slanted tip angle of 23°. A high voltage was applied between the capillary and the cathode placed facing the emitter to obtain a steady continuous spray having properties similar to the cone jet mode of an electrospray. The spray was illuminated using a diverging laser beam normal to the spray and was examined in real time using a CCD camera microscope. Figure 4.2 (a, b) illustrates the stable cone jet mode like spray obtained. When viewed from the top as in Figure 4.2 (a), the spray was found to be symmetric about its axis (in red) and the axis of the capillary tube (in black). However, when viewed from the side as illustration in Figures 4.2 (b), it was noticed that the axis of the symmetric spray (in red) is parallel to the cross sectional surface of the emitter rather than the axis of the capillary tube (in black). This spray phenomenon was found to occur irrespective of the rotation of the capillary tube along its axis and thus probable cause due to gravity was found to be negligible in the spraying mode obtained.
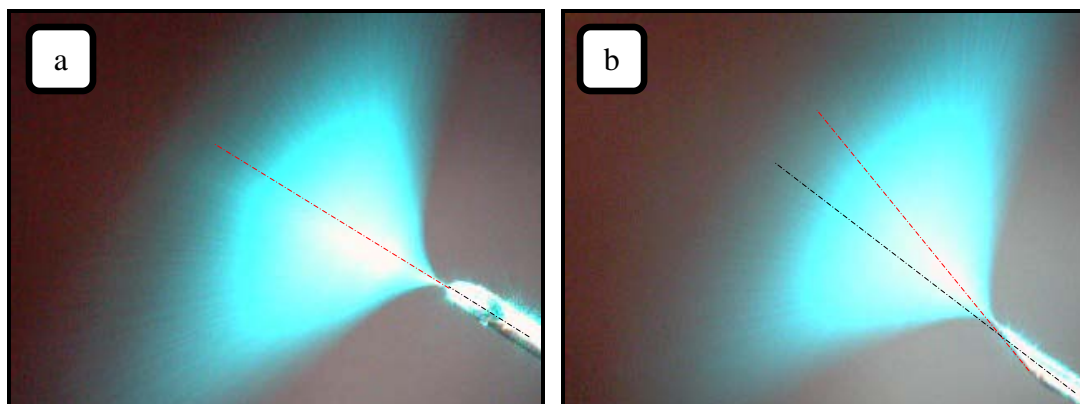
Figure 4.2 Spray profile illuminated using laser beam. Shown profile is viewed from a) top and b) side. Good symmetry and stable spray profile are noticeable

The experiment was repeated using a higher viscosity fluid, i.e. ethylene glycol having viscosity 19.9 mPas [22] (whereas viscosity of ethanol is 1.16 mPas) and the input voltage was adjusted to obtain a stable spray. However, it was hard to operate the spray in a cone jet mode. Either the spray was steady, abnormally shaped and coaxial to the capillary tube axis as depicted in Figure 4.3 or, with increasing voltage the spray turned to multiple jets with their axis parallel to the cross sectional surface of the emitter.
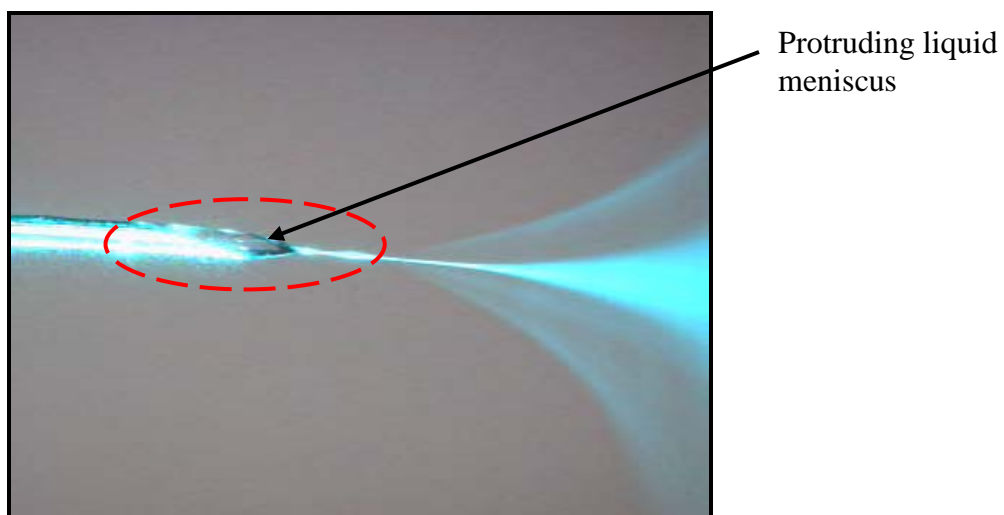

Protruding liquid meniscus

Figure 4.3 Stable spray of ethylene glycol obtained using slanted emitter tip

The type of spray generated is determined by the meniscus formed at the emitter tip. When a flat ended emitter is used, the meniscus formed has a semispherical shape and deforms at the pole due to electrical forces forming a jet. The meniscus formation when using a slanted capillary tip using a low viscosity fluid (ethanol) and a high viscosity fluid (ethylene glycol) was studied. When the viscosity of the liquid is increased, it was found that the meniscus formed was semispherical in shape as shown in Figure 4.4(b) which undergoes electrical shear forces to generate the spray. Whereas, lower viscosity fluids smear around the cross sectional surface of the emitter and form a spheroid meniscus at the apex of the emitter as shown in Figure 4.4(a). The reason for the difference in meniscus formation could be attributed to the inherent viscosity and surface tension of the fluids.
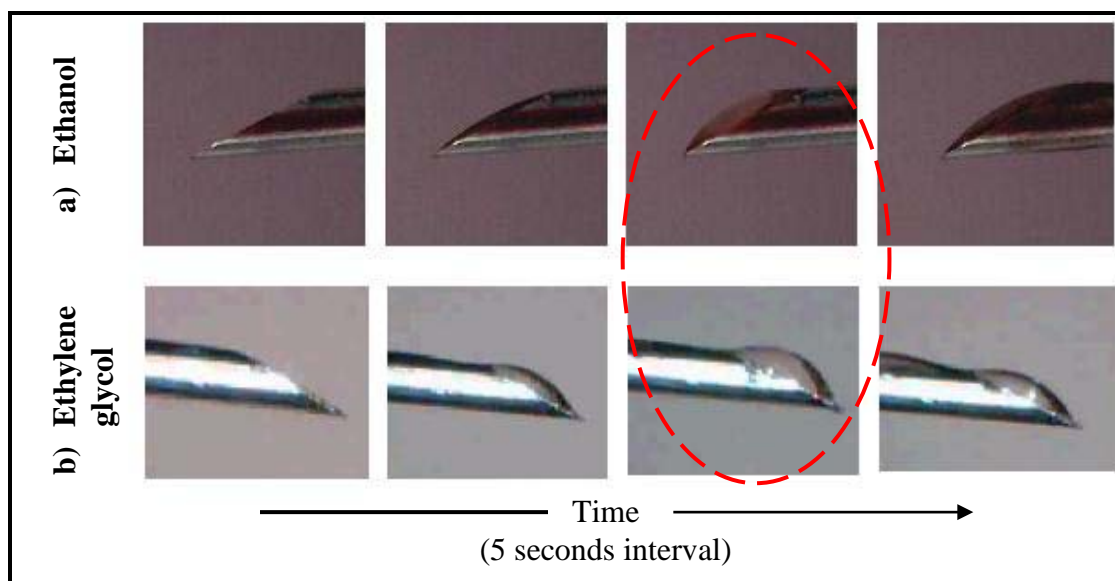

Figure 4.4 Comparison of meniscus formation in ethanol and ethylene glycol. Note bulge in meniscus formation for ethylene glycol and smeared meniscus in ethanol

Consequently, it was found that the direction of the generated spray could be controlled by changing the cross sectional angle of the emitter tip. The following finding was useful as the nanoparticles ink solution could be sprayed onto a substrate surface normal to the laser pattern, without the emitter being coaxial to the projected laser pattern. Although the spray obtained illustrates the stable and axis symmetric properties of operating in the cone jet mode, it differs from traditional definitions of a cone jet mode since,

- In the cone jet mode, the spray direction obtained is parallel to the emitter axis and sprays normal to the emitter cross sectional surface

- The type of emitter used is considered an irregular profile and the modes of spraying in such geometries have not been classified

4.2. INVESTIGATION OF FLOWRATE

Experimentally it was found that the voltage required for extracting an ink solution increased with increase in flowrate. The same was established from literature [27, 28] where the relationship between flowrate and voltage was found to be linear. Although studies have been performed describing the effects of flowrate on voltage, film size formed and emitter diameter, an understanding on any apparent change in the shape of spray geometry and density distribution within the spray is uncertain. This experiment was performed using the apparatus setup shown in Figure 4.1. The experiment was conducted by flowing ethanol and ethylene glycol as the ink solution. A syringe pump was used to regulate the flow between 2µl/min and 8 µl/min with an increment of 1 µl/min. The spray was allowed to elapse until a constant stable spray was obtained before

the profile of the spray was imaged. The experiment was repeated for different trials by changing setup parameters including a change in the fluid used to ethylene glycol, type of extractor used and location of the extractor. Trends were observed for spray length, spray size and laser beam intensity for changing flowrate while examining the microscopic images and are illustrated in Figure 4.5. The trends were found to occur in all the different spray trials mentioned.
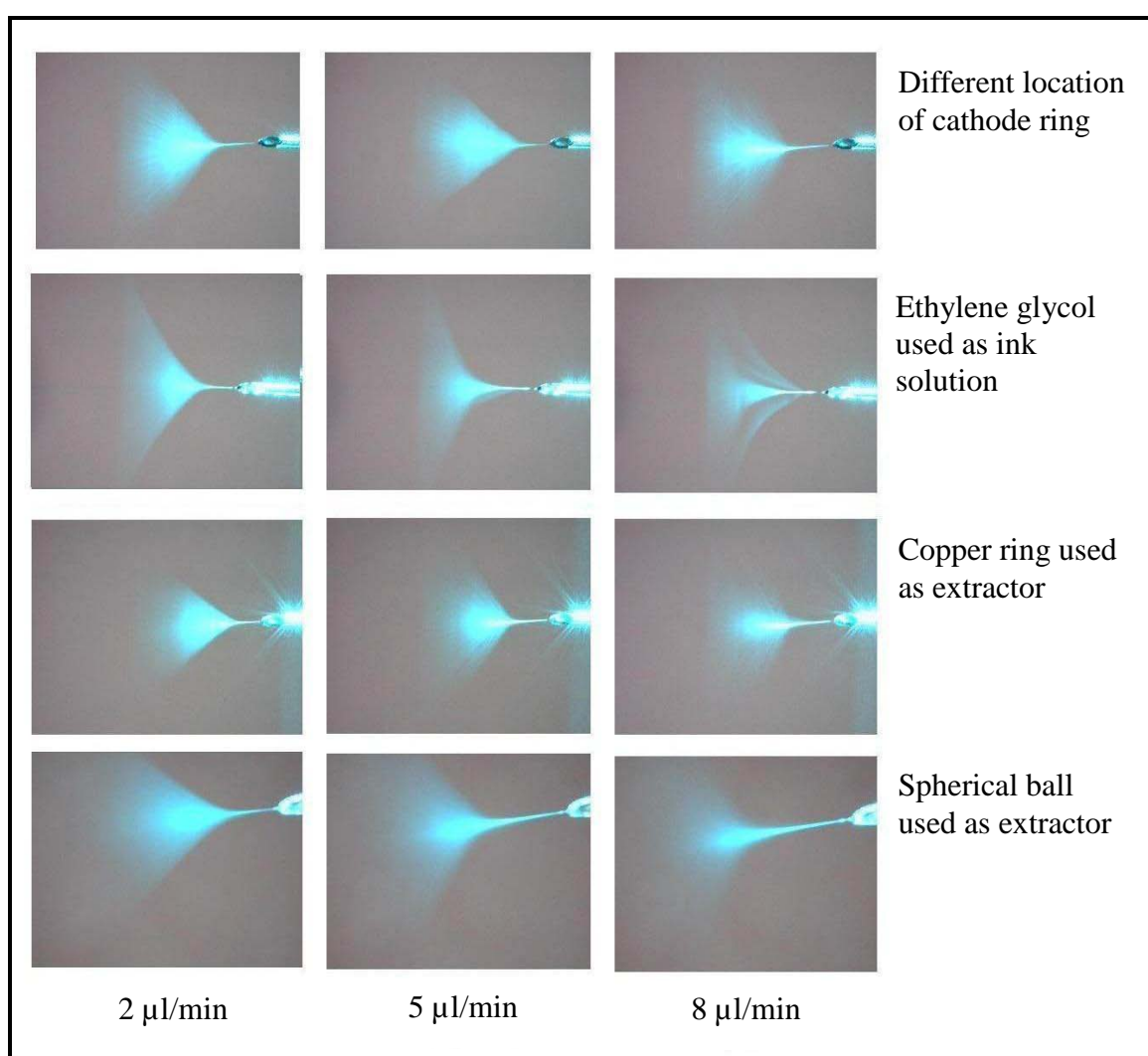

Figure 4.5 Observed variations in jet length and spray density for different flowrates. Note changing illumination size and jet length in all trials for different flowrate

On examining the spray profile images taken using the CCD camera microscope, length of the jet was found to increase with increasing flowrate. The size of the spray core is observed to be decreasing whereas the reflected laser beam intensity is observed to be increasing for greater flowrates. To improve the visibility of small differences, the image was enhanced using image analysis software ImageJ. The original images were processed by a sequence of image processing operations. First, the background from the original image was subtracted and the edges of the spray were detected. A lighter background was then added to the obtained image to increase the contrast between the different regions of the spray. The enhanced images for a single trial are shown in Figure 4.6 and are interpreted in detail.
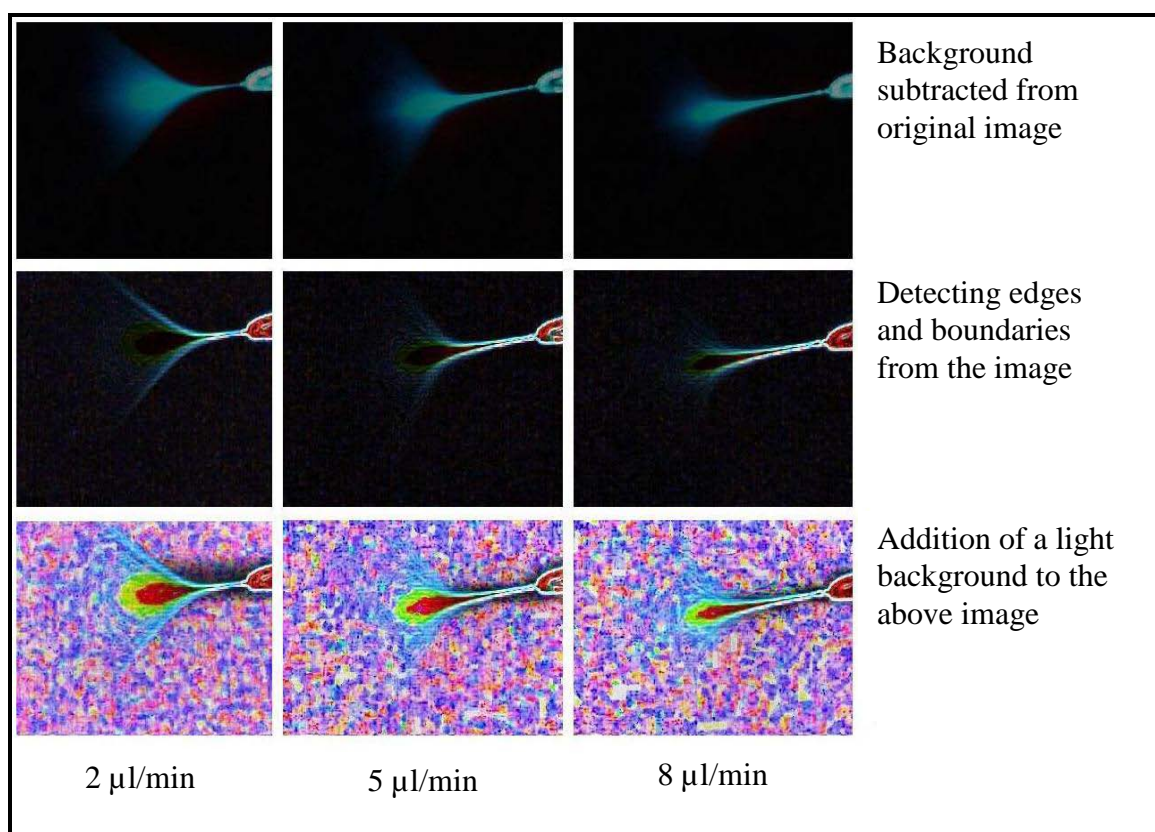

Figure 4.6 Enhanced images comparing spray for different flowrate

The length of the jet (distance from the emitter tip to the spray core, i.e. region in red) is seen to increase with flowrate. Observing the spray core, it is found to reduce in width while increasing in length for increased flowrates. The thickness of the core boundary (shaded in green) is noticed to be diminishing in size with increased flowrate. Finally, the core region seems to change from circular in shape into an elliptical contour. Although the variation in color intensities could be used to study the dispersion of the spray, the advancement of the findings has been restricted due to a possible discrepancy in the experimental setup. It is unclear whether the shape and size of the core obtained was caused due to the spot size or profile intensity of the laser beam. Thus it is possible that the colored core and trailing edges of the spray would not be providing a true representation of the spray profile and density specifically at higher flowrates where the jet length is greater. This could be overcome by using a suitable lamp source having a much larger spot size than the spray. The variation in distribution within the spray could be examined using the core size and color. However the illumination source would have to be calibrated to avoid inaccuracies due to varying illumination intensity of the source.

As an advantage, with increased flowrates greater number of nanoparticles can be deposited onto the substrate. Increasing jet length would facilitate easier apparatus setup but the current supplied to the spray would have to be minimized to reduce the radius of nanoparticle distribution.

4.3. INVESTIGATION OF ELECTRIC FIELD

The variation in spray characteristics was observed by changing the configuration of the electric field. The electric field was changed using different sizes of the cathode

ring as the extractor and displacing the cathode. Initially the substrate was located between the emitter and extractor but for practical applications, the extractor was placed before the substrate. Presence of a substrate in between the emitter and extractor was found to weaken the electric field and subsequently higher extraction voltage was required. The weakening of the electric field was overcome by placing the extractor ahead of the substrate.

The diameter of the cathode used is represented by φ_c and the displacement of the cathode is represented by Δ_c. A thin copper rod was wound into rings having diameters 0.75, 1 and 1.5 inches and was mounted onto a fixture made from an insulating material. The location of the cathode was moved along the direction of the axis of the capillary with the emitter tip as the reference plane. The cathode ring was displaced ahead (+) and past (-) the emitter tip. The setup is illustrated in Figure 4.7.
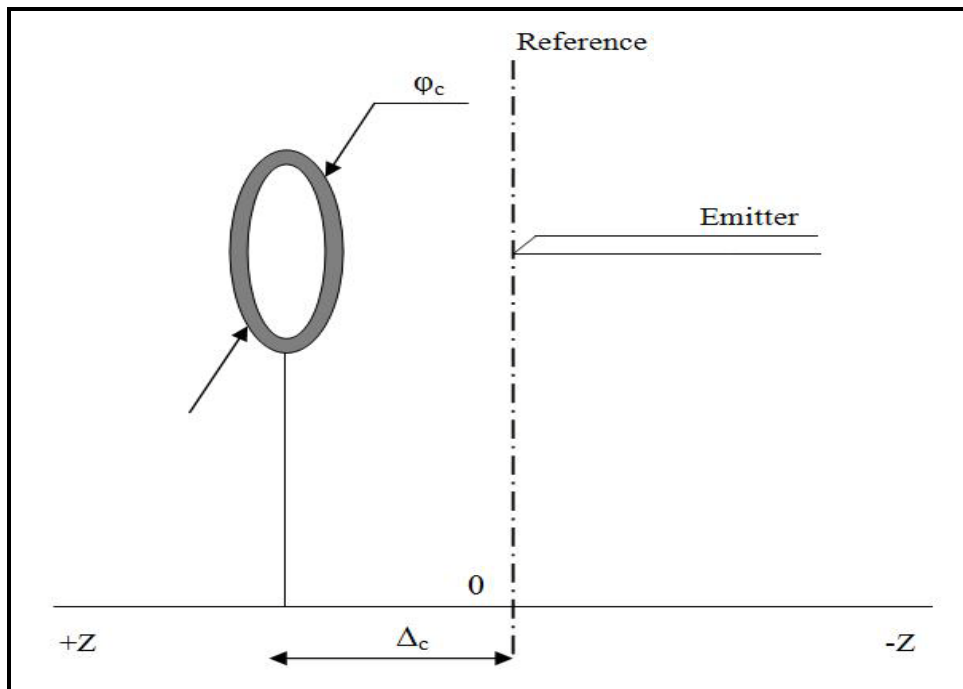

Figure 4.7 Setup used to study influence of varying cathode size and location

The change in spray is tabulated in Figure 4.8. When the cathode ring was placed past the reference plane (-), the spray formed tends to curve backwards causing a widely diverging spray. The size of the core was found to increase with decreasing cathode diameter. While the cathode was placed away from the emitter, the length of the jet was found to increase with increasing distance of the cathode location. Very minimal difference is seen with decreasing cathode sizes.
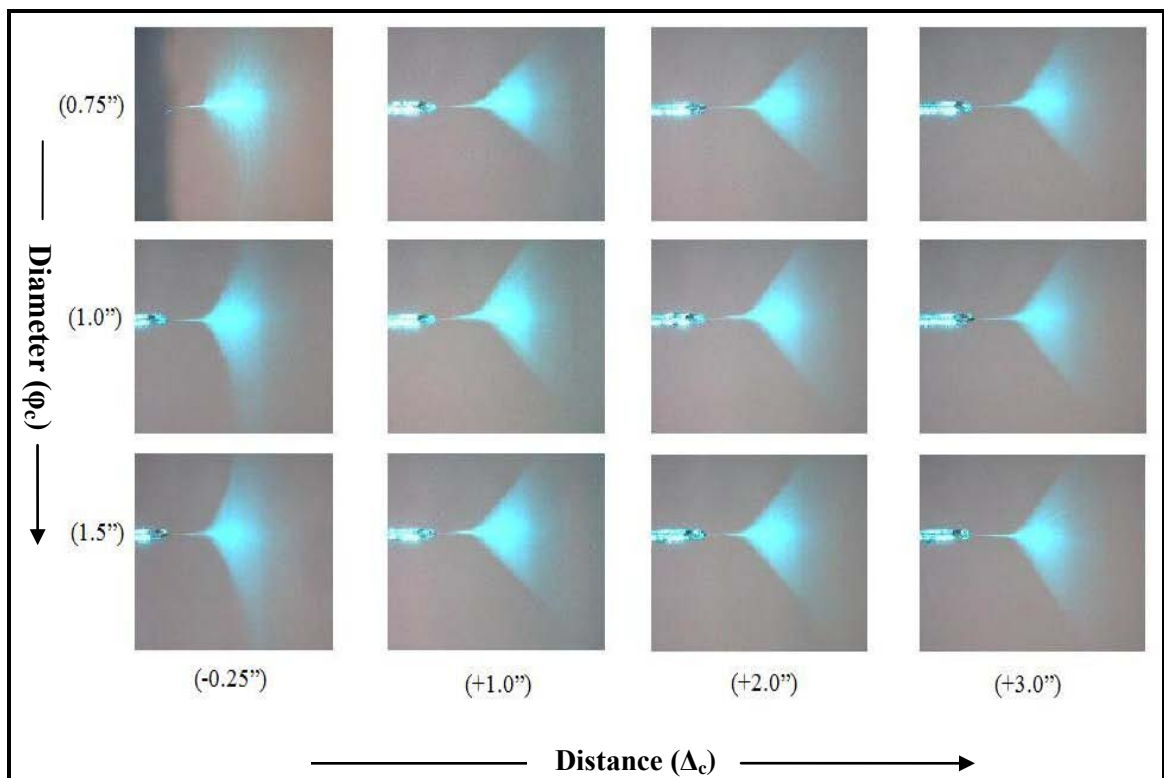

Figure 4.8 Observed change in spray by varying cathode size and location

In a second experiment similar to the above experiment, an investigation was conducted by supplying a high voltage to an anode ring rather that the emitter. From literature, it has been reported that during reverse polarity, the spray does not differ vastly

with exception to that it was found to be choppy and uneven. The anode was placed past

(-) the reference plane and the cathode was placed ahead (+) of the reference plane. Here

φ_a and Δ_a represent the diameter and the displacement of the anode respectively. The

experimental setup is shown in Figure 4.9.
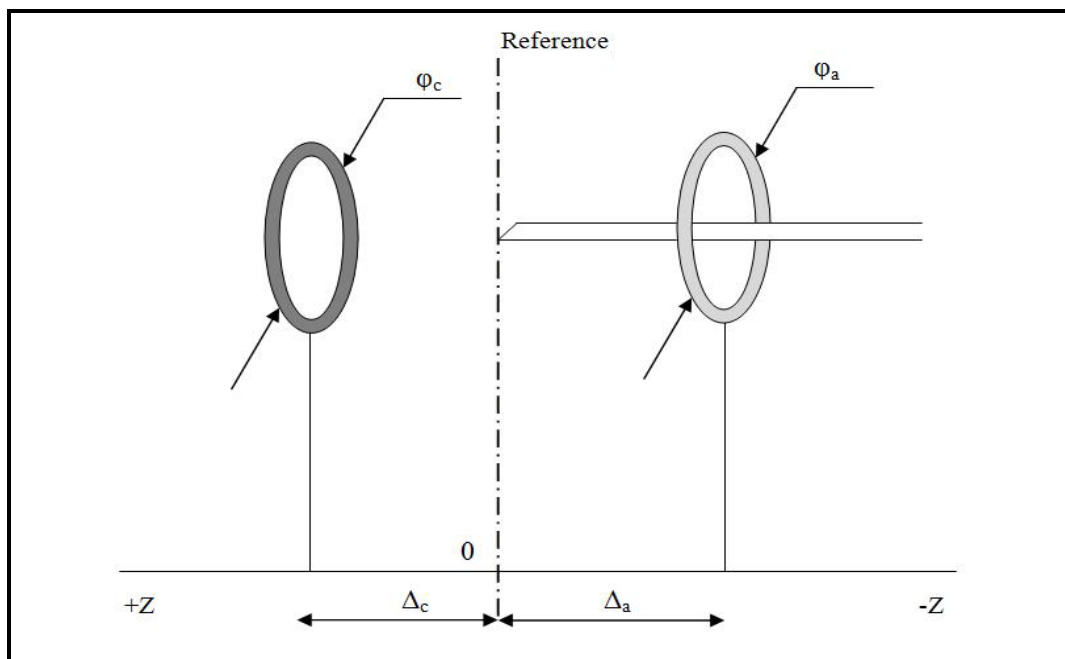
Figure 4.9 Setup used to study influence of varying anode and cathode size and location

The input voltage required to generate the spray was found to have increased

considerably. The spray obtained seemed to be directed backwards towards the anode

rather than the cathode as seen in Figure 4.10 and becoming sharper with decreasing

anode diameter. The probable cause of the spray was due to the anode having a greater

influence on the spray than the cathode. When the cathode was moved closer to the

anode, the voltage required for the spray reduced and the spray became normal

resembling the cone jet.
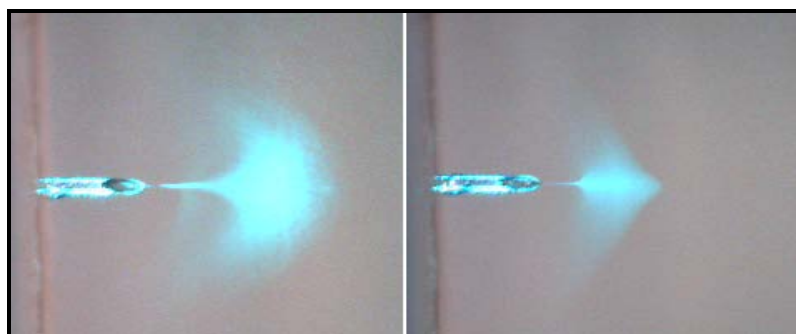
Decreasing diameter size of ring

Figure 4.10 Spray having anode positively and cathode negatively displaced

When the anode and cathode were placed ahead (+) of the emitter, a stable smooth spray was formed. The spray is illustrated in Figure 4.11. The spray was found to be narrower with decreasing size of the anode ring. The spray was repeated by interchanging the position of the anode and cathode. The spray was obtained independent of the polarity of charge and unaffected by location of the electrode distant from the emitter tip. Although the spray obtained was highly suitable for nanoparticles deposition, it was impractical to use the setup since the input voltage supplied to the electrodes was limited by the maximum input voltage of the high voltage power supply.
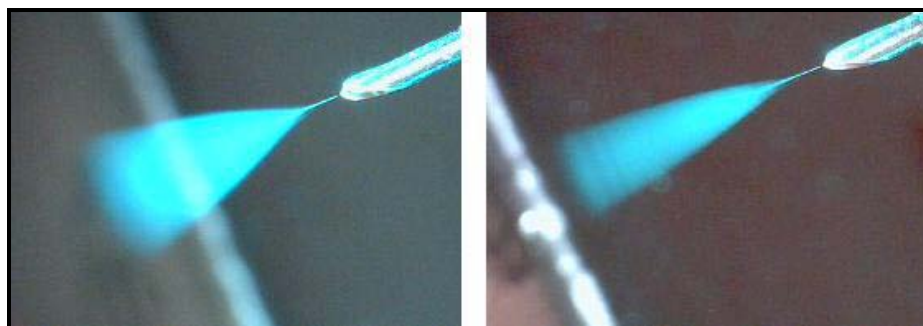
Decreasing diameter size of ring

Figure 4.11 Spray having anode and cathode positively displaced

4.4. WASHING AND RIM FORMATION

Distance between the emitter surface and the deposition substrate, i.e. standoff distance was found to have an influence on the deposition of nanoparticles on the substrate. When the distance between the emitter and the substrate was relatively close, liquid droplets settle onto the substrate and cluster together to form larger droplets. These droplets are washed aside by following droplets that impact the wet nanoparticles on the substrate. This leads to the effect where the nanoparticles on the surface are washed away towards the edges and agglomerate around the spray as shown in Figure 4.12. During long periods of spraying as the size of the deposition grows in thickness, droplets were found to impact the surface of the deposition due to reduced standoff distance. When the distance between the emitter and the substrate is increased, the washing away effects are found to die out. Thus standoff distance was found to have an influence in the deposition and washing of nanoparticles from the substrate surface.
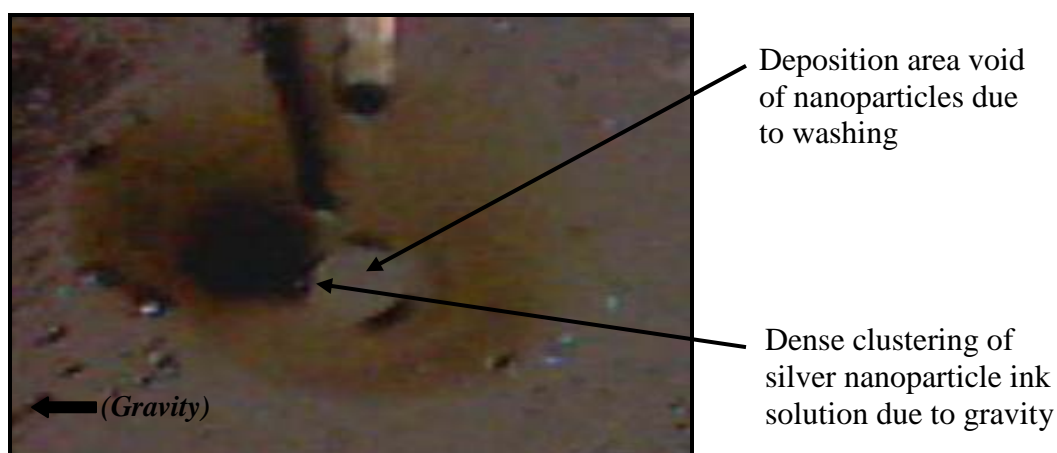

Figure 4.12 Disturbance of nanoparticles during deposition due to washing

During sintering, provided the deposited nanoparticles exist as a thin layer of liquid solution like in the case of washing, rim like formation were observed. The resulting micro structure formed consists of nanoparticles that are agglomerated and sintered onto the perimeter of the pattern as shown in Figure 4.13. The high power of the laser beam, which is focused at the ink solution containing nanoparticles, raises the temperature locally at the exposed region rapidly resulting in a decrease in surface tension. Thereby, nanoparticles in the solution are dragged toward the colder outer region by thermocapillary forces creating rim-type elevations at the edges of the pattern. Figure 4.13 (a) depicts a triangular rim elevations formed during a deposition whereas Figure 4.13 (b) depicts an elevation formed by a circular laser pattern. Sintered depositions inside the elevated rim like deposition are noticeable but are very small in size. The formation of rim like elevations can be eradicated by reducing the laser power of the projected pattern or the amount of liquid solution present in the deposited nanoparticles.
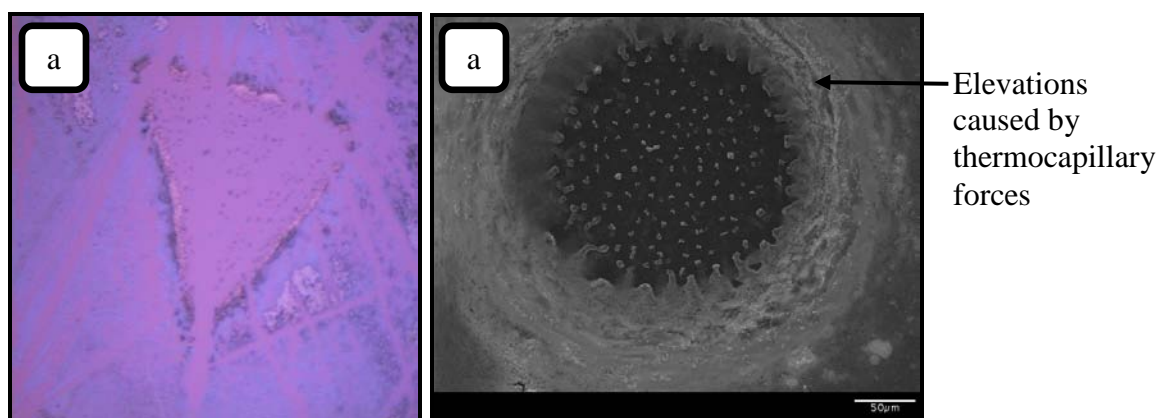

Figure 4.13 Rim formations during nanoparticle sintering. Note the rim like elevations of sintered nanoparticles along perimeter of projected pattern due to high laser power, a) triangular pattern and b) circular pattern

4.5. DESIGNED EXPERIMENT OF COMBINED PARAMETERS

Design of experiments (DOE) was used to study the relationship and combined influence of the parameters previously found to influence the spraying of nanoparticles, more specifically the width of the nanoparticle spray. A three factorial experiment was designed for studying the influence of flowrate (A), cathode diameter (B) and displacement of the cathode (C). The factors were varied at two levels (High, Low) with a center point (Mid) as described in Table 4.2.

Table 4.2 Parameters used in the designed experiment

Fluid used: 200% Proof Ethanol	A. Flowrate	B. Diameter cathode	C. Distance cathode
2 levels	υ_o	φ_c	Δ_c
3 factors	µl/min	Inch	Inch
1- LOW	2	1	0.5
2- MID	5	1.5	1
3- HIGH	8	2	1.5

A specially designed fixture consisting of prearranged slots to affix the cathode location was made to facilitate ease and repeatability in conducting the experiments. The fixture was combined to the existing apparatus setup described in Figure 4.1 to conduct the experiments. From prior experiments, the high, low and mid value settings for the DOE were selected. A set of random sequences were generated to randomize the operational procedure of the designed experiment and each experiment was randomly replicated for a total of three runs. The three factors were varied and the response of the spray was recorded. A total of 10 experiments were run with 8 experiments having high - low settings for the input factors and 2 midpoint settings for the input factors.

Although the width of the spray was measured as the output response, the output of each experiment was acquired as images. The experiments were run and the spray formed was allowed to stabilize before three sequential images were taken at an interval of 5 seconds each. In order to maintain consistency in measurement, width measurements were taken from the captured images using image analysis software ImageJ. The images were combined into a stack or temporarily related images with each image being a slice from the stack. By processing a single image slice, the complete stack could be processed. A rectangular box of width of 3 pixels and height of the image was drawn over the image at a known pixel value from the trailing (left) side of the image. The external region from the rectangular area in the image was cleared. The captured and processed images are shown in Figure 4.14. In the processed image (Figure 4.14b), the shaded spray area was treated as a particle and the major and minor diameter of an ellipse fitted over the particle was used to identify the width of the spray. The major diameter of the ellipse was instituted to be the width of the spray. The operations performed on a single image slice are exactly replicated for the stack of 90 images to obtain the response for the output.
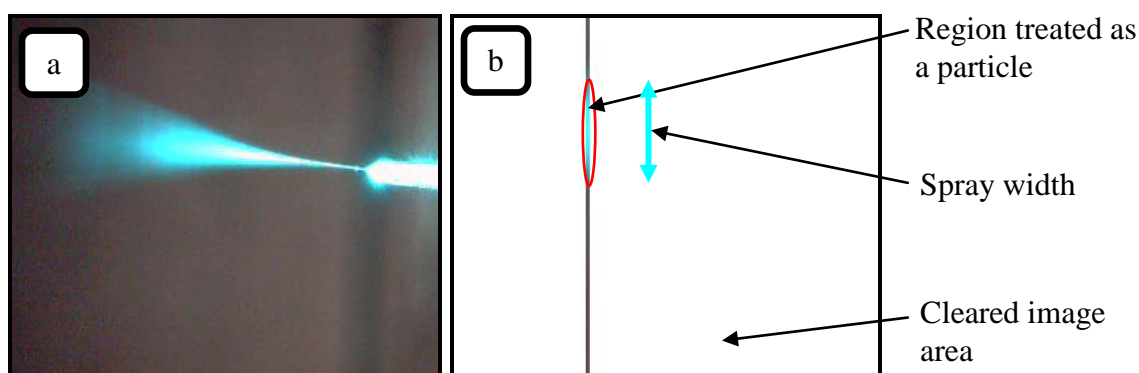

Figure 4.14 Example of width measurement using ImageJ. Images shown depict the a) captured image and b) processed image for a single image slice

The measured spray width was analyzed and interpreted using Design of Experiments software, Design Expert. P-values from the analysis of variance (ANOVA) shown in Table 4.3 indicate the significant factors that contribution to the model. Flowrate and displacement of the cathode were found to be most significant in the DOE model. Diameter of the cathode ring and interaction between the factors were not found to be significant. Residuals for the ANOVA were normal and randomly distributed indicating that the factors assumed were reasonable and the model is appropriate.

Table 4.3 ANOVA of the designed experiment

Source		Sum of Squares	DF	Mean Square	F Value	Prob > F	
Model		1853.97	2	926.98	42.47	0.0007	Significant
	A	1584.85	1	1584.85	72.61	0.0004	
	C	269.12	1	269.12	12.33	0.0171	
							Not significant
Curvature		129.61	1	129.61	5.94	0.0598	
Residual		109.13	5	21.83			
Cor Total		2092.7	8				

The model F-value of 42.47 implies the model is significant. There is only a 0.07% chance that a "Model F-Value" this large could occur due to noise. Values of "Prob>F" less than 0.0500 indicate model terms are significant. Values greater than 0.1000 indicate the model terms are not significant.

In conclusion, minimum spray width was found to be at maximum flowrate and at smaller distance between the extractor and the emitter. Coefficients were used to construct the model equation to predict output responses for different factor values and are represented by the equations below,

$$\text{Spray width} = +79.98333 - 4.69167 A*\text{Flow} + 11.6C \tag{4.1}$$

$$\text{Spray width} = +79.98333 - 4.69167*\upsilon_o + 11.6 \Delta_c \tag{4.2}$$

5. MODIFIED DEPOSITION APPARATUS

5.1. PROPOSED MODIFICATIONS

The primary change in the apparatus was the elimination of the electrospray aerosol generator. It was replaced by an electrospray setup placed right before the substrate such that the obtained plume of nanoparticles is directly deposited onto the substrate. This eliminated the need for a carrier gas to transport nanoparticles to the substrate. Use of a carrier gas would result in increasing the diffusivity of the nanoparticles and the velocity of the gas would determine the probability of nanoparticles temporarily adhering or rebounding from the substrate surface.

Secondly, the flow of nanoparticles and the laser pattern were made coaxial making use of an emitter having an irregular profile, i.e. a slant angle. From experiments, it was found that the spray generated was parallel to the slanting surface of the emitter. Thus the emitter was to be placed offset to the laser beam and the direction of the spray was controlled by the slant angle of the emitter. The resulting spray generated by the modification was coaxial to the laser beam pattern.

Finally, a cathode ring was introduced ahead of the substrate to extract the nanoparticle ink solution from the capillary tube. Based on the result from the designed experiment, the ring was placed slightly ahead of the emitter nozzle. Although the diameter of the cathode ring was found to play no significant role in the spray, the voltage required to extract fluid was found to increase with diameter. Thus the size of the ring was maintained to be small enough to be fit within the setup and operate at lower voltages but large enough to prevent sparking between the emitter and the extractor.

5.2. PROTOTYPE SETUP

Silver Nanoparticles having a mean diameter of 30nm (from Sumitomo Electric) was added to ethyl alcohol (Acros Organics, absolute, 200% proof) in the ratio of 1%, 2% and 5 % by weight to produce a nanoparticle ink solution. The mixture was stirred and subjected to ultrasonic vibrations to obtain a homogeneous solution free of agglomerated silver nanoparticles. A known amount of the nanoparticles ink was pumped into the setup using a microprocessor controlled syringe pump (KD Scientific). Ink is sprayed onto the substrate incident to where the laser beam is focused by applying a high potential between the emitter and the extractor. A copper wire having thickness of 600 microns was wound into a ring and was used as the extractor. The substrate is placed vertically on a horizontally traversing stage (National Aperture). The setup is enclosed in a box to prevent contamination by nanoparticles. The environment inside the box is cleaned by flushing compressed air into the chamber and venting the exhaust contaminated air into an in-line Teflon gas filter (Entegris Wafergard) having a removal rating of particles greater than 0.003µm or 3nm.

The nanoparticles were sintered using a patterned laser beam. A 5W Argon-Ion laser (Spectra-Physics, multiple wavelengths from 454 nm to 514 nm) was used to produce the laser beam. The emitted laser beam is expanded by passing through a 5X beam expander (Edmund Optics) and is projected onto the micromirror array of a DMD (Texas Instruments, 800*600 pixels). The DMD serves as an array of reflective aluminum micro-mirrors which can be tilted to form angles of either ±10° with respect to the surface. When the micro-mirror is in -10° state, it is classified as ON and conversely, when the micromirror is in +10° state, it is classified as OFF. Patterns of the structure

were created in PowerPoint slides, which were then executed using the DMD to generate a dynamic mask. The illuminated light is modulated according to the defined mask. Illumination from the micromirror surface is either reflected towards the light sink or an objective lens. The individual mirrors are either turned ON or OFF depending upon the pattern drafted on the input slide. Mirrors that are in the ON state produce a reflected laser beam of the deposition pattern and is focused into a few micrometers in size using a long working distance objective lens (Mitutoyo, 10X) onto the substrate. The prototype setup is shown in Figure 5.1.
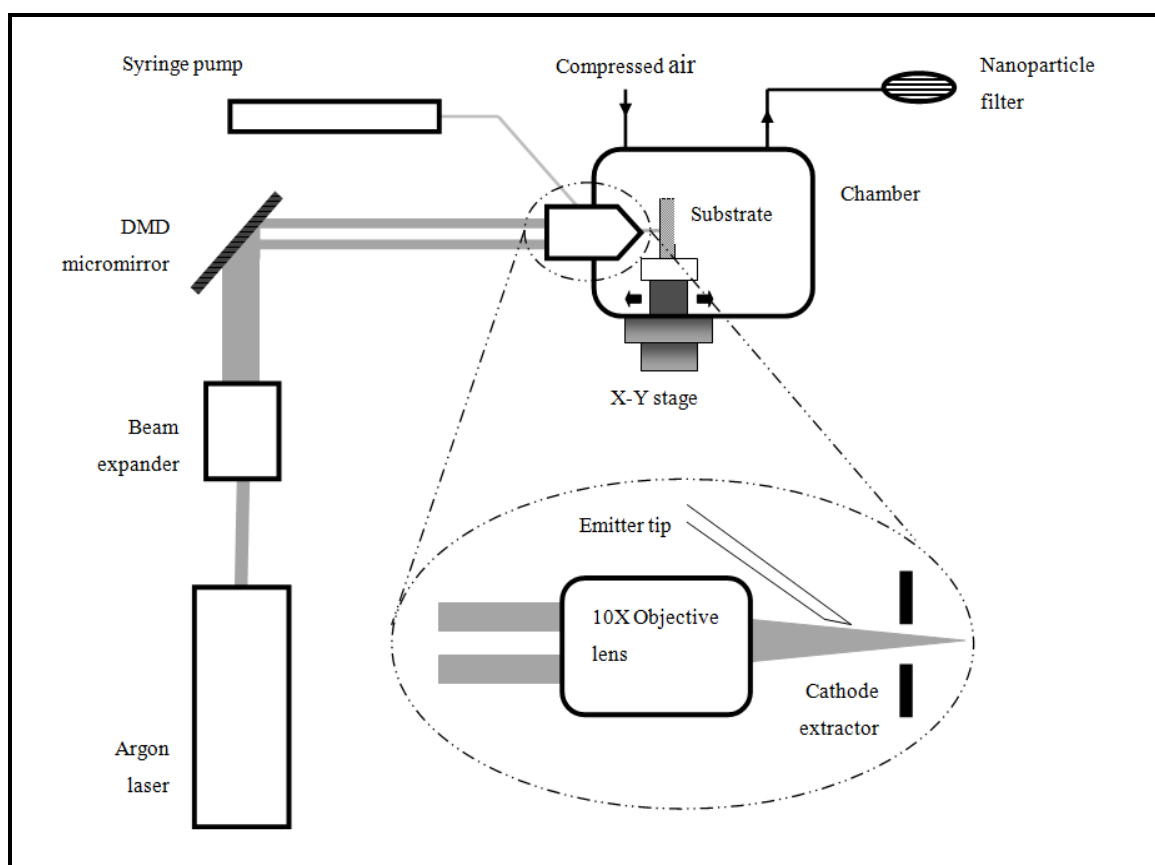

Figure 5.1 Apparatus setup for deposition using modified spraying process

5.3. OPERATIONAL PROCEDURE

The nanoparticles ink solution is extracted from the emitter by applying a voltage between the emitter and the extractor. The voltage applied to the setup is adjusted until the spray obtained is operating in a steady state cone jet mode. The ethanol present as small droplets in the spray evaporates due to its low boiling point and elevated temperatures leaving behind a plume of finely dispersed silver nanoparticles. A piece of silicon wafer is cleaned by washing in water and is rinsed in ethanol. Excess liquid is forced off the surface using a canned air duster and mounted onto the holder. The standoff distance for the spray is experimentally adjusted in advance to prevent the phenomenon of washing from occurring on the substrate. Silver nanoparticles from the plume are deposited onto the substrate.

During impact with the substrate, the adhered nanoparticles are loosely bonded to the substrate surface due to surface tension. To ensure complete bonding of the nanoparticles in the required shape, a laser pattern is used to heat the nanoparticles and sinter them. Two dimensional patterns of the geometry are input into the micromirror array and the generated laser pattern is focused onto the partially bonded silver nanoparticles on the substrate. The illuminated area is sintered under the laser beam exposure. By repeatedly spraying nanoparticles and exposing them to the laser pattern, the thickness of the microstructure is increased. The substrate is then washed in ethanol to remove the unexposed and loosely bonded nanoparticles from the substrate leaving the bonded pattern behind.

6. EXPERIMENTAL DEPOSITION RESULTS

6.1. SURFACE DEPOSITION OF NANOPARTICLES

The transportation and deposition of nanoparticles onto a substrate using the electrospray aerosol generator previously used was examined. Using nitrogen as the carrier gas, nanoparticle deposition trials were conducted using the electrospray aerosol generator to deposit nanoparticles onto silicon and glass substrates. The velocity of the carrier gas used was found to be vital in the placement of nanoparticles. During operation in the cone jet mode, no evident depositions or agglomorations were found on the substrate. Rather than the cone jet mode of electrospraying, in a microdripping mode where small spherical droplets are extracted form the emitter, depositions were observed when using a low flowrate of carrier gas. With a higher flowrate of carrier gas, no evident formation of nanoparticle depositions were observed.

The deposit formed were found to have elevated edges consisting of a large number of nanoparticles whereas the central inner surfaces was thin with a reduced concentration of nanoparticles. The depositions formed without supplying a carrier gas is depicted in Figure 6.1. From the SEM image Figure 6.1(a), the agglomoration of nanoparticles on the outer circumference indicate an effect similar to washing which is caused by the presence of ethanol since the spray obtained is in tiny agglomorations of droplets. Within close proximity of the aerosol generator exit, sequential droplets were found to overlap over one another as shown in Figure 6.1(b). It is evident that nanoparticles cluser at the edges of the droplets creating a trough like uneven surface. With increasing distance between the aerosol generator and the substrate, the droplet deposition was found to diverge.
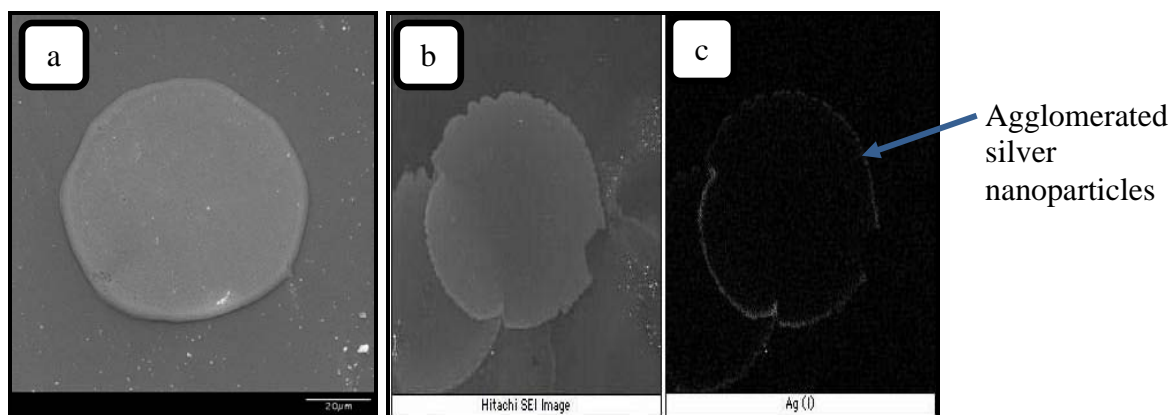
Figure 6.1 Nanoparticle deposition obtained using the electrospray aerosol generator. Images a; b) SEM images and c) phase map, show the agglomoration of nanoparticles at the boundray of the droplet

To identitify the randomness of the ink droplet motion, the nanoparticles were sprayed and observed by placing a glass slide from the expulsion end of the electrospray aerosol generator. Figure 6.2 illustrates the random directions in which the droplets are emitted as seen on the glass slide where the nanoparticle agglomorations are highlightened in red boxes. In general, at close proximity to the emitter, droplets repeatedly overlap over one another. At increasing distances, the droplets diverge towards random directions as in Figure 6.2. Finally at very larger distances, the agglomoration become unnoticable.
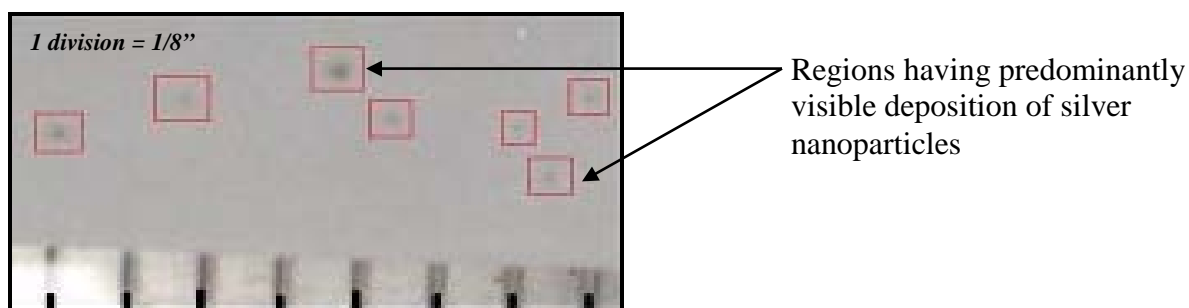

Figure 6.2. Nanoparticle agglomoration on a glass slide. The particles were deposited using the electrospray aerosol atomizer

To transport nanoparticles over a long distance, the carrier gas should be a laminar flow to avoid nanoparticle diffusion as they tend to follow gas streamlines. Carrier gas at low flowrates was ineffective in transportation as the nanoparticles were deposited onto the flow tubing ahead of the substrate. Higher flowrates cause the nanoparticles to diffuse and would require a specific mechanism (such as aerodynamic lenses) to collimate the nanoparticles. Increased flowrate also increased the number of particles that rebound on collision with the substrate. Although aerodynamic lenses were considered to collimate nanoparticles, they would be difficult to setup with a coaxial laser beam due to their large size and operational mechanism. Alternatively, the nanoparticle transportation system and laser beam could be arranged at a slight angle from each other. But this would require calibration of the offset component. Moreover, from literature it is known that aerodynamic lenses are designed considering the transported particle material density and hence, an aerodynamic lens system could be ineffective to focus different metallic and nonmetallic nanoparticles.

In order to easily deposit nanoparticles onto the substrate, the electrospraying process was located closer to the substrate. When the spraying process occurs close to the substrate surface, nanoparticles are directly deposited onto the substrate. The absence of a carrier gas helped reduce the number of nanoparticles bouncing away on collision with the substrate. The electrospray was operated in a cone jet mode to obtain a fine plume of nanoparticles. The sprayed nanoparticles were deposited onto a substrate directly placed at close proximity to the trailing end of the spray. A well distributed thin layer of nanoparticle deposition was produced. The formation of a thin layer of silver nanoparticles on a silicon substrate is shown in Figure 6.3.
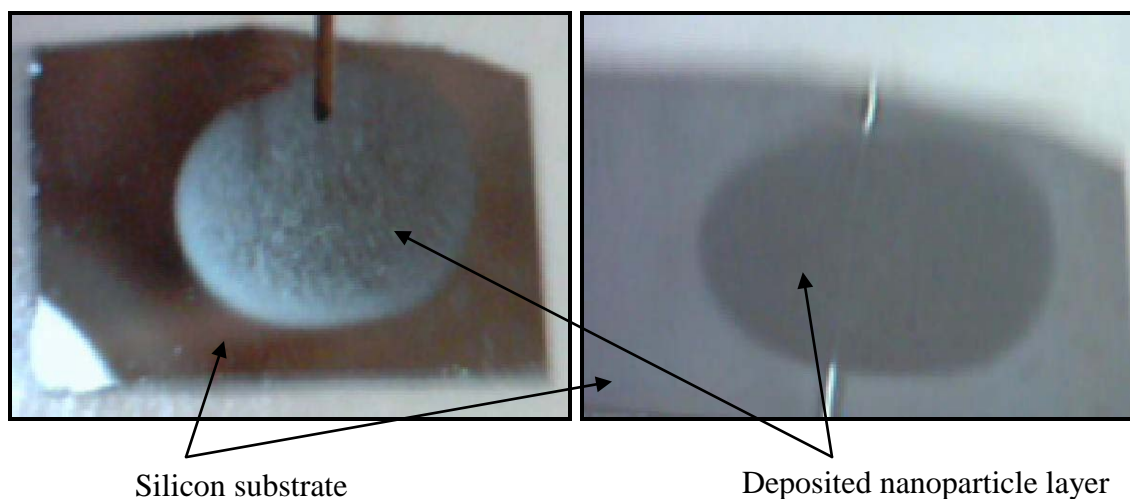
Silicon substrate   Deposited nanoparticle layer

Figure 6.3 Deposition of silver nanoparticles on silicon substrate. The deposition was obtained by directly electrospraying silver nanoparticles substrate and formation of good thin layer is observed

A thin layer of nanoparticles was deposited onto the substrate using the modified setup. The cross sectional area of the emitter surface was kept normal to the substrate and a silver nanoparticle ink solution was sprayed in the cone jet mode. The deposited nanoparticles were found to be located at a predefined location. Visual examination of the deposition demonstrates that the deposition is a flat thin film of nanoparticles without edge concentrations or large agglomerations. The diameter of the obtained deposit was found to be about ¼" with a slight increase in diameter for prolonging deposition time. The diameter of the spray obtained could probably be controlled by changing the flowrate of the ink solution.

In conclusion, an easy and effective method to deposit a thin layer of nanoparticles at a predefined location without the need of a coaxial system or offset calibration was identified. The depositions of nanoparticles could be easily replicated by directly spraying nanoparticles and the observed deposition layer is superior for microstructure fabrication than using an electrospray aerosol generator.

6.2. NANOPARTICLE DISPERSION – IMAGE ANALYSIS

The deposition of nanoparticles onto the substrate surface was examined to study the deposition formation, its shape, dispersion and roughness through image analysis. The electrospray apparatus was arranged according to the modified prototype and silver nanoparticles were sprayed onto a silicon wafer. The spraying of nanoparticles was captured using a CCD camera microscope placed facing the deposition surface. A substrate was placed in front of the spray and the deposition process was recorded. Images were sequentially extracted from the recorded deposition process at equal time interval of 2, 5, 10 and 30 seconds. A series of obtained images are shown in Figure 6.4 and the images were processed using image analysis software ImageJ.
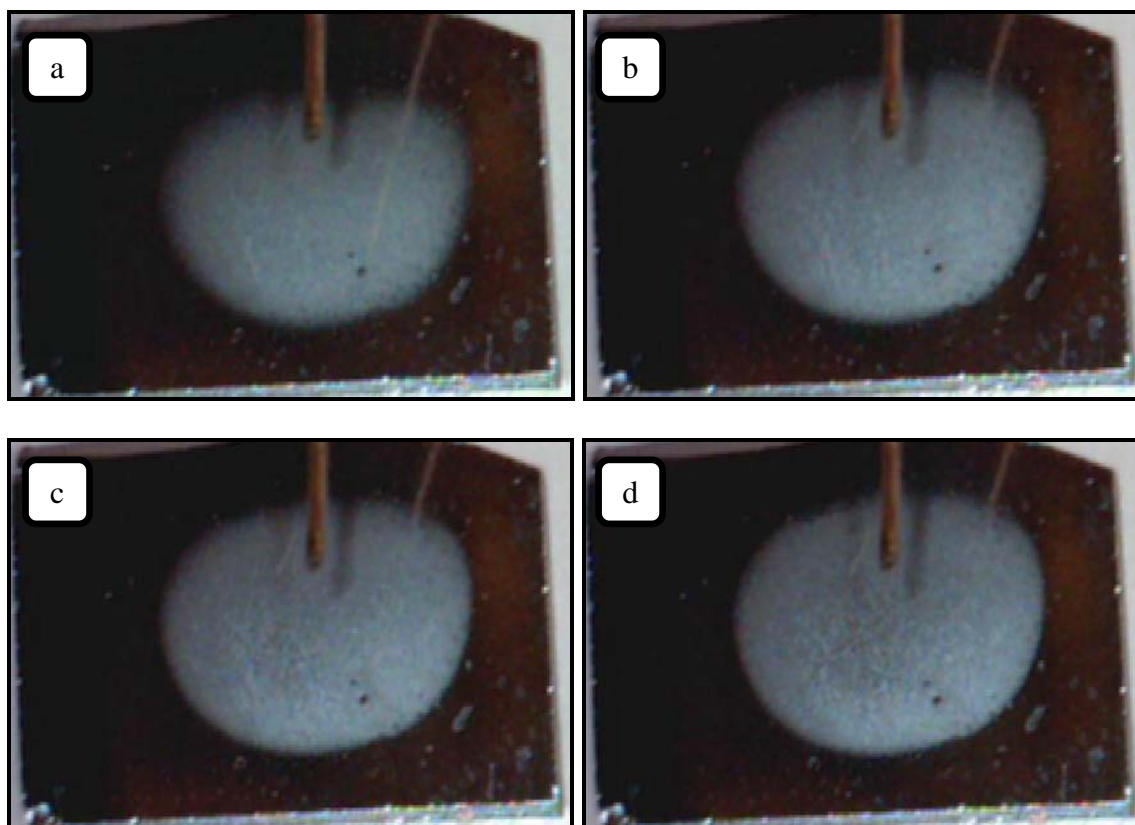

Figure 6.4 Extracted deposition images. Each taken at 10 second interval from (a) to (d)

The extracted images were sorted in the order of sequence taken and uploaded to the analysis software. The images were cropped (enclosing the deposition region alone) to reduce and avoid the distortion caused by the image background and changes in light intensities due to reflection from the substrate surface. The images were converted to grayscale images, i.e. images composed of shades of grey, varying from black (weakest intensity) to white (strongest intensity). The intensity of the light is obtained from the individual pixels in the image. Two dimensional surface profiles and three dimensional surface plots were generated by the software based on the grayscale value of individual pixels. For the 2D profile, sequential images having time interval of 5 seconds were extracted. A line of width 1 pixel and appropriate length covering the deposition area was selected. The profile was generated using the software by plotting the intensity of the individual pixels on the line against the pixel distance from the starting point of the line. The obtained 2D profiles of the deposit are shown in Figure 6.5.

A platykurtic distribution (lower rounded peak than a normal distribution and shorter thin tails) of nanoparticles was initially observed in the surface profile illustrated in Figure 6.5 (a). Comparing the individual profile plots, the height (grayscale value) of the profiles increase from Figure 6.5 (a) to Figure 6.5 (c) whereas the width of the deposit (distance in pixels) is found to be constant. Judging by the change in profile, the final deposition of nanoparticles can be said to be a polydisperse distribution. The slight negative skew (elongated tail on the left) observed on the plots is caused due to the tilt in the axis of the microscope camera in relation to a normal from the substrate.
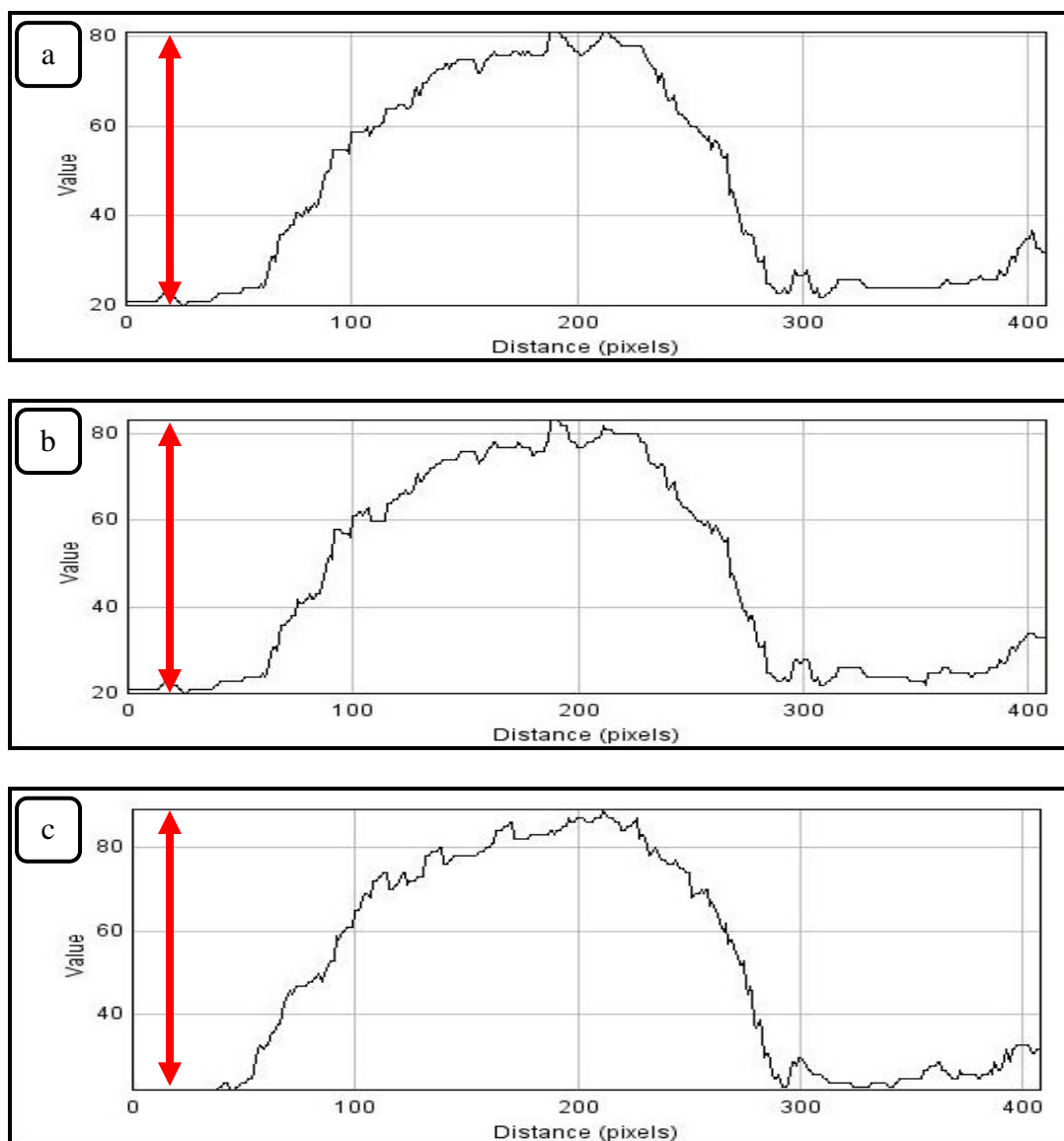
Figure 6.5 2D surface profile of nanoparticle deposition. Note the size variation of the profiles generated from images at time interval of 5 seconds each from (a) to (c)

Three dimensional surface plots were generated using the software by plotting the intensity of individual pixels over an area (region enclosed by a rectangular box instead of a line) against the pixel distance of each pixel along two axes. The surface plots generated were more like having a series of 2D profiles placed successively. The generated plots are shown in Figure 6.6 with each image taken at 20 second interval.
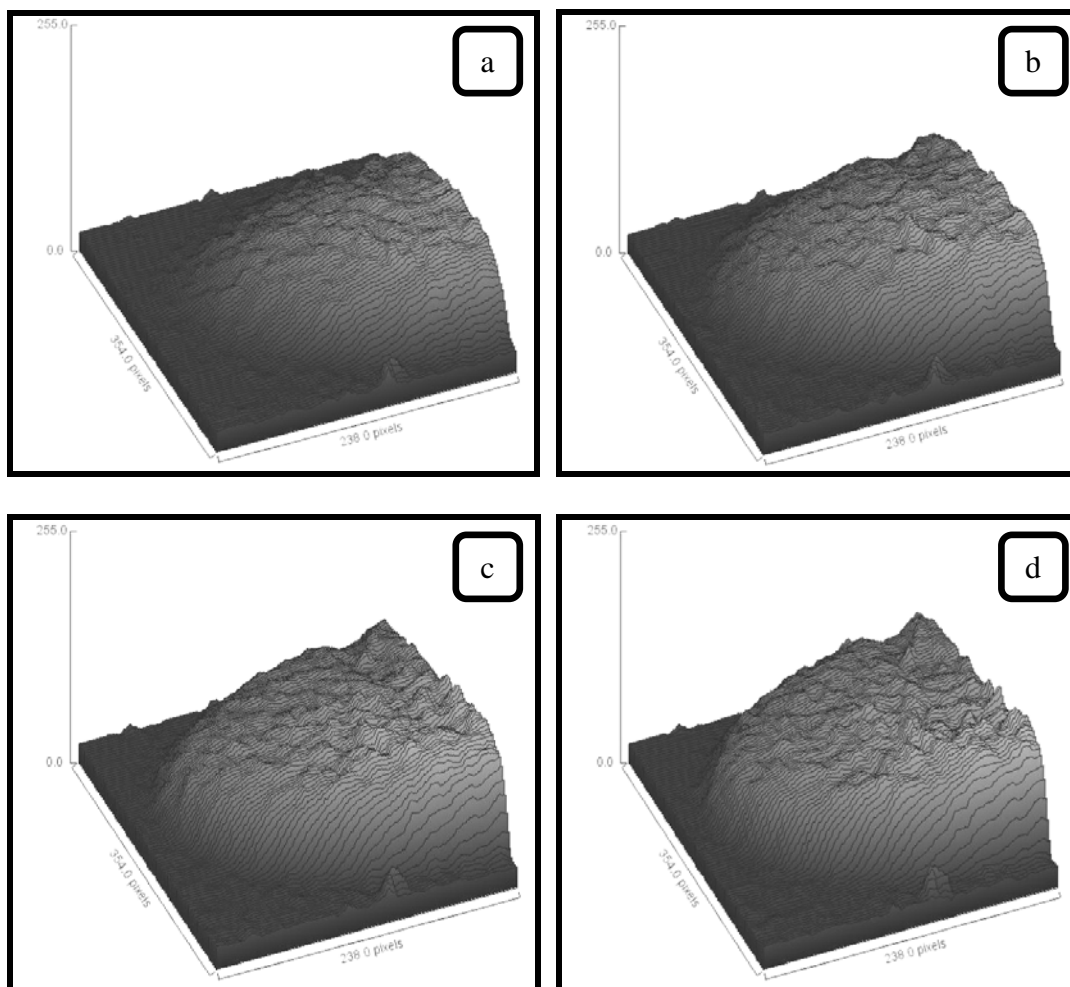
Figure 6.6 3D surface plots of nanoparticle deposition. Note the surface change in plots generated from images at time interval 20 seconds each from (a) to (d)

Parallels can be drawn in inference made from the 3D plots and the 2D profiles. The initial surface plot Figure 6.6 (a) shows the deposit formed to be a platykurtic distribution. With increasing layers of nanoparticles Figures 6.6 (a) to (d), the deposition was found to grow greatly in thickness and minimally in radial size. Visually, larger depression and unevenness on the upper surface of the deposit are observed in later plots as in Figure 6.6 (d) relative to plot Figure 6.6 (a) indicating a rise in the roughness of the surface with deposition thickness.

Using luminance (grayscale value) of the pixels shaded by yellow in Figure 6.7 as data points for height, a superimposed 2D profile was drawn for the nanoparticle deposition process taking sequential images having 10 seconds interval. For the initial plots, in Figure 6.7 (a) to (d), a clear defined profile illustrating the cross sectional profile shape was generated. For subsequent images (not shown), the profile generated was erratic having grayscale values below the previous generated profile. Practically, nanoparticles do not diffuse at such rates and hence the profile would be erroneous. As the height of the deposit increases, the captured images get blurry (out of focus) resulting in the erratic behavior of the profile. Such images were omitted.
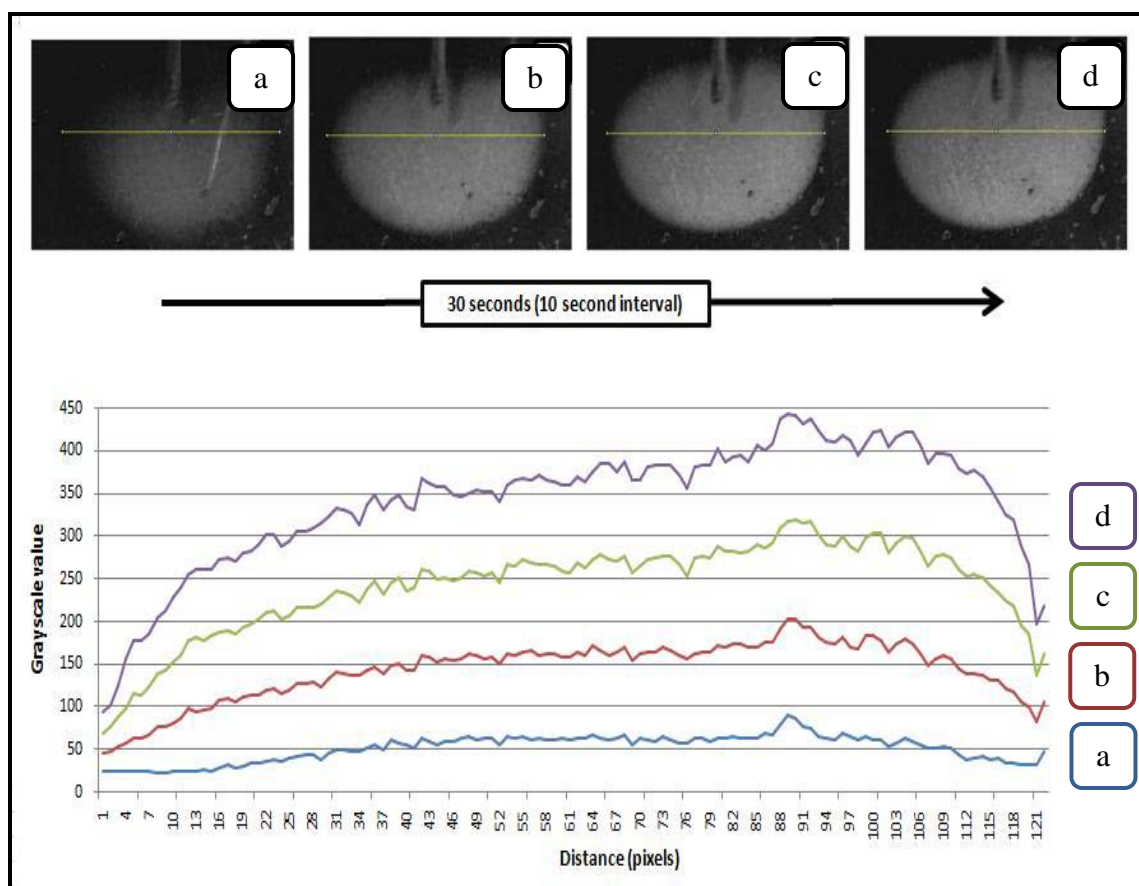

Figure 6.7 Superimposed 2D profile of nanoparticle deposition

A fair idea on the roughness of the deposited nanoparticles could be observed from the image analysis. As the deposition layer becomes thicker, increasing deviations are noticed between the two profiles shown in Figure 6.8. This is inferred as the increase in roughness with nanoparticle deposition. At the edge of the deposit, increase in the deposition height of particles and consistent radial distance are noticed. The region outlined (in red) shows a steeper angle formed at the edge. Finally, it can be concluded that the distribution of nanoparticles starts as platykurtic and progresses to become polydisperse (on the surface) with a Gaussian tail.
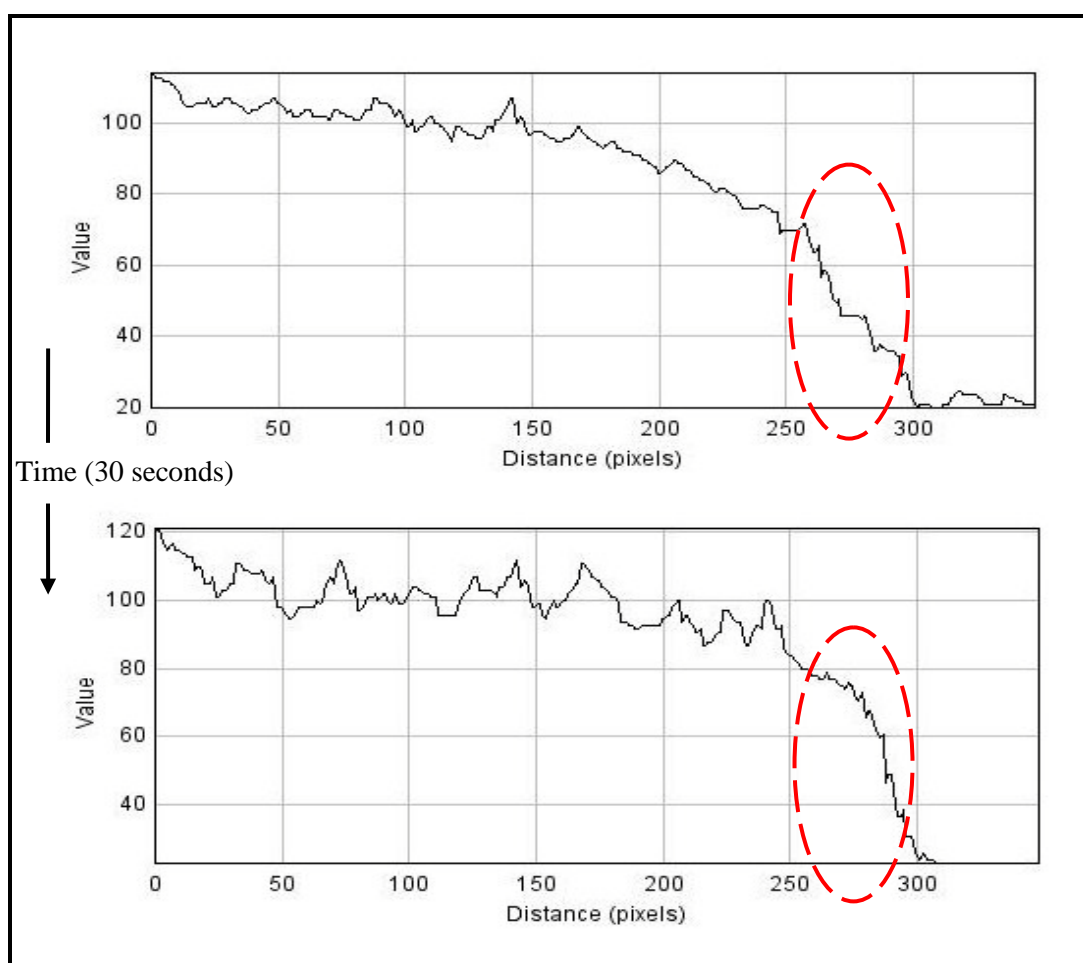

Figure 6.8 Profile comparison of deposit periphery

6.3. NANOPARTICLE DISPERSION – MICROSCOPY ANALYSIS

Silver nanoparticles were sprayed onto a silicon substrate to deposit a small layer of nanoparticles. The particles were sintered with the laser beam to prevent diffusion of nanoparticles into the atmosphere. The deposit surface was examined under an optical microscope to study the distribution of the deposited particles. Distinct regions of nanoparticle deposition were easily identified and are shown in Figure 6.9. The deposit consisted of a circular dense concentration of nanoparticles at the center and rapidly fading towards a lighter concentration of nanoparticles towards the borders. At the edge of the deposit, a thin ring consisting of lightly concentrated particles surrounding the center of the deposit pattern is observed with a rapid change in color from darker reddish brown core to a lighter blackish brown ring. The steep change in color and the small border ring width surmise with high confidence that the dispersion of nanoparticles follow a polydisperse distribution as observed by image analysis.
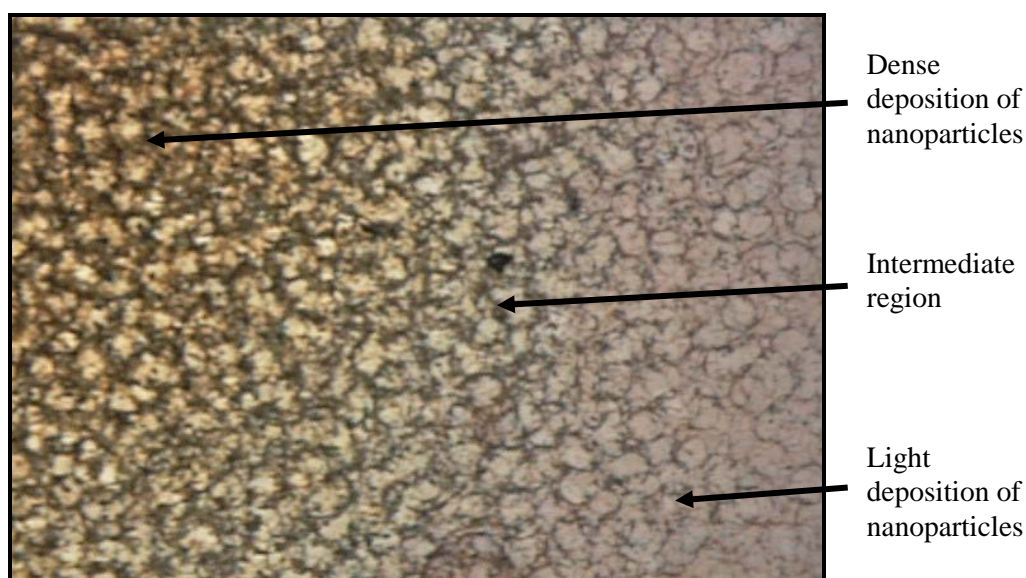

Figure 6.9 Optical microscope image of deposit pattern. Note the distinct change in color and density

The deposit surface was examined under an atomic force microscope isolated from external vibrations. The surface of the microstructure obtained was found to have a large number of clustered nanoparticle protrusions, depressions and voids creating a large variation in surface height. The obtained microstructure and surface variation is shown in Figure 6.10 and Figure 6.11 for different areas of deposition. In the current process, a low powered laser beam was used to sinter the nanoparticles together. In the process, these nanoparticles were heated to about 150°C to undergo expected partial melting on the surface and bonding between the particles was made through necking. A layer is formed by necking of several nanoparticles on the surface.
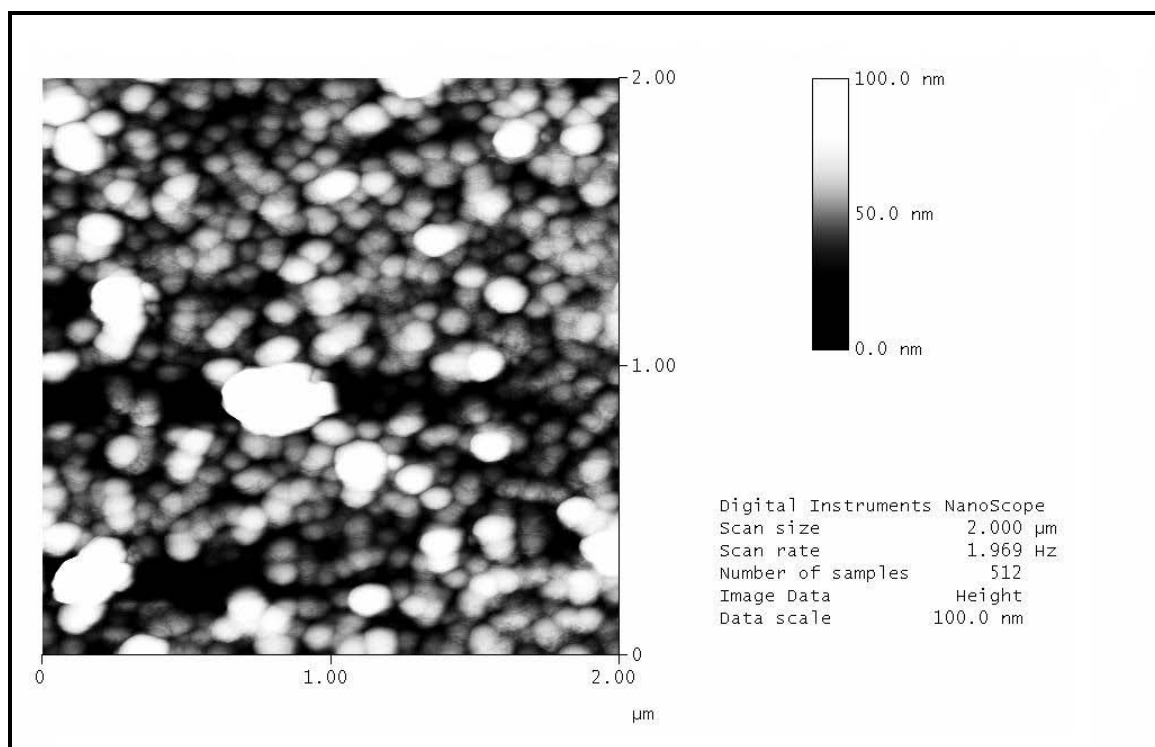

Figure 6.10 AFM image of deposition surface (4µm^2 area). Image illustrates the neck formation mechanism between individual nanoparticles and the range of deposition layer thickness over the substrate
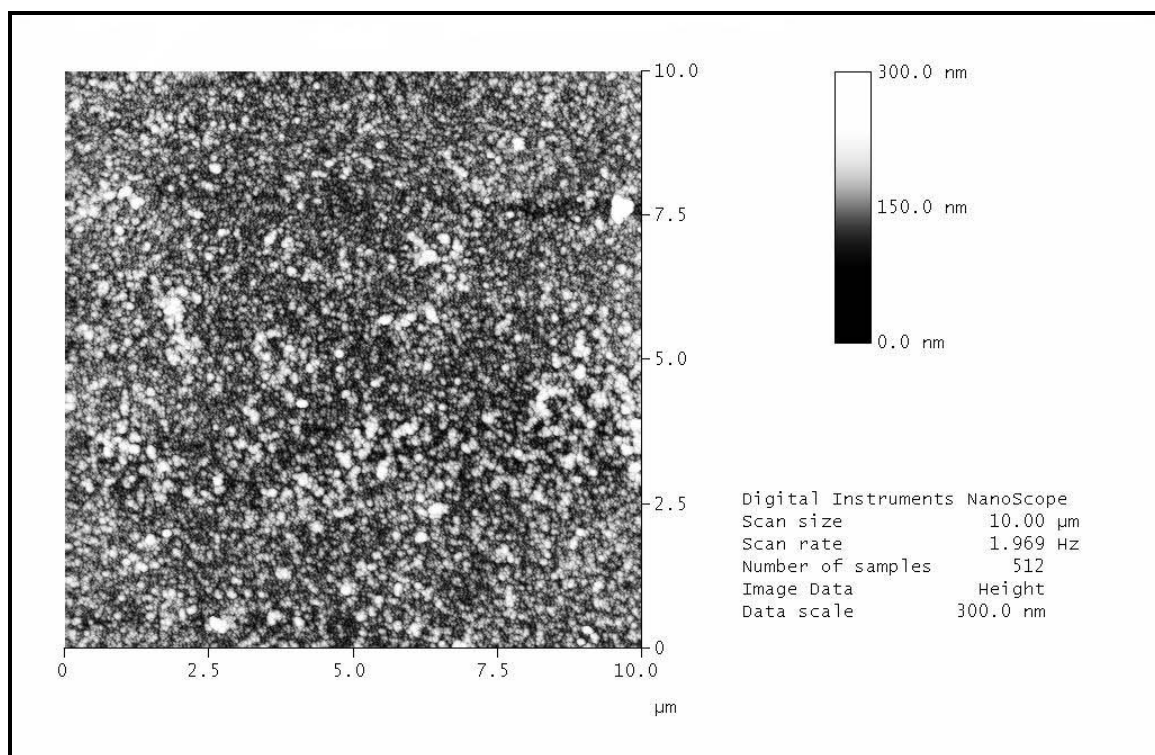
Figure 6.11 AFM image of deposition surface (100μm^2 area). Roughness and depth of the deposition layer is observed

The predominant presence of nanoparticle protrusions and depressions over the surface could be due to presence of liquid solvent (ethanol) with the nanoparticles during sintering which was done to prevent the diffusion of particles during observation using an atomic force microscope. However, such surface variations could be minimized by heating the nanoparticles to higher temperatures where the particles are nearer to complete melting which would cover depressions and reduce protrusions. Temperatures provided in literatures are in the range of 450°C to 500°C for complete melting to occur. Reaching such high temperatures is currently limited by the laser used and the microstructure deposition process. Post deposition annealing in a furnace or using a higher powered laser beam can be used to smooth the microstructure layer.

6.4. LASER SINTERED MICROSTRUCTURES

Microstructures consisting of silver nanoparticles were deposited onto a silicon wafer using the proposed deposition setup. Modulated laser beam (pattern I) shown in Figure 6.12(a) was focused onto the substrate while nanoparticles were simultaneously deposited onto the substrate. Microstructures were replicated on different silicon substrates for different laser pattern exposure time. The sintered deposition was rinsed in ethanol to remove unexposed and loosely bonded nanoparticles from the surface, air dried and examined under an optical microscope. Shown in Figure 6.12 (b, c and d) are the formed microstructures. Features were found to be well replicated like the chamfer between the lines and the sharp edges. The patterns were measured to be roughly 500 by 500 micrometers in size and their varying sizes was due to the change in focal length caused between setups.
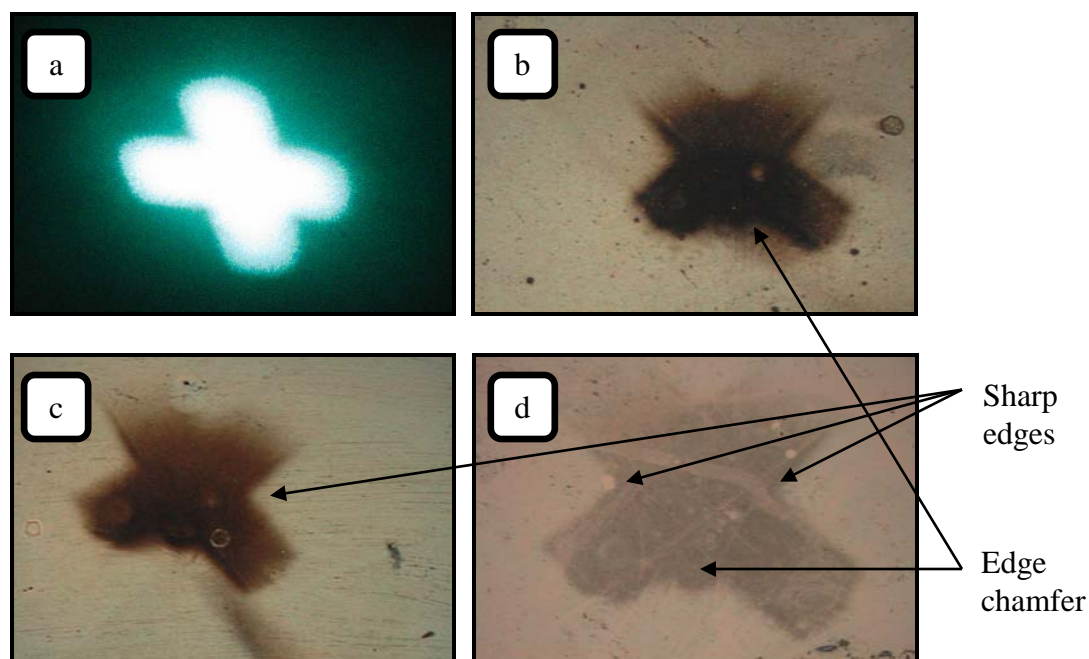

Figure 6.12 Sintered microstructures, pattern I. Shown are the a) laser pattern and b; c; d) optical images of microstructures. Clearly visible are the reproduced sharp features

The microstructures were examined using a scanning electtron microscope. The individual nanoparticles were found to have agglomorated into larger particles with pattern I, see Figure 6.13(a and b). At high magnifications, visible are the bonding of the agglomorated nanoparticles with each other caused due to necking. The microstructure deposition does not cover the entire surface of the exposed pattern and has areas completely void of nanoparticles or agglomorations of nanoparticles having large porosities between the agglomorated globules.
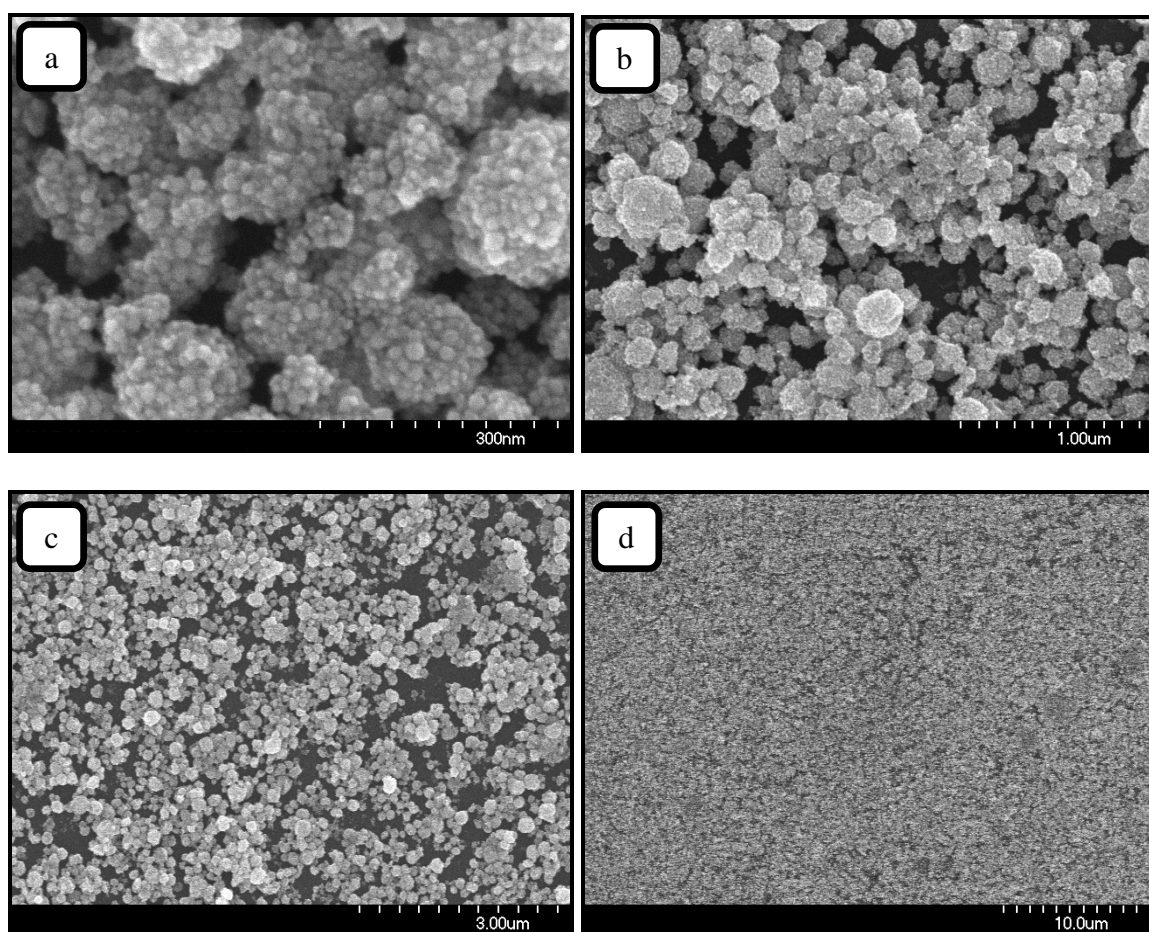

Figure 6.13 SEM images of sintered microstructures, pattern I. Images show the a; b) bonding of individual nanoparticles and c; d) deposit layer of nanoparticles

Similarly, another microstructure was fabricated by sintering silver nanoparticles onto a silicon substrate. A different laser pattern (pattern II) was focused onto the deposited nanoparticles on the substrate and the microstructure is shown in Figure 6.14. The primary difference in obtaining the following microstructure compared to the earlier fabrication was the change in parameters to have higher number of nanoparticles deposited onto the substrate and increased duration of laser exposure. Size of the microstructure was found to be roughly 800 by 800 micrometers.
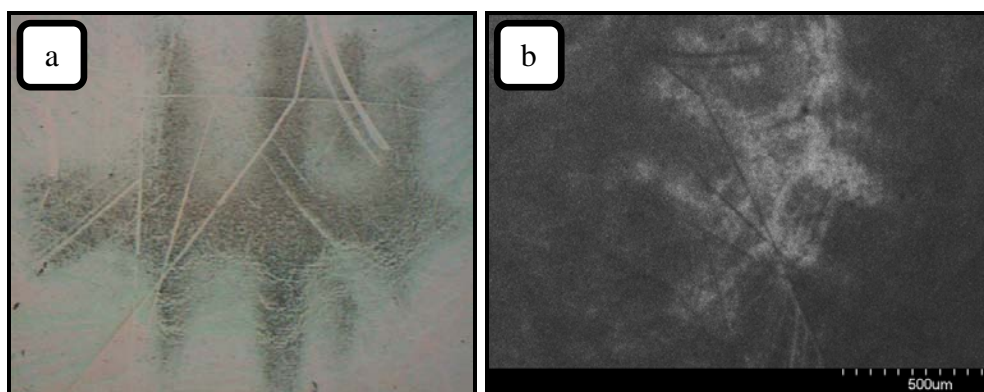
Figure 6.14 Sintered microstructures, pattern II. Shown are a) optical image and b) SEM image, of the deposit pattern having increased number of nanoparticle layers

These depositions were observed to have a different surface structure compared to the previous microstructure depositions (Figure 6.13). Examined microscopic images of the microstructure are shown in Figure 6.15. From Figure 6.15 (a), the bonding of individual nanoparticles is found to transpire due to necking, like the previous microstructure. However the layer formed in the current microstructure consists of a continuous mesh like layer having nominal nanoparticle protrusions and depressions while the previous microstructure formed had ball like agglomerations with large protrusions and empty spaces. From Figure 6.15 (b), the coverage of nanoparticles over

the silicon substrate can be observed. The nanoparticles are found to cover a majority of the surface with respect to the previously deposited microstructure where large voids are found between agglomerated nanoparticles.
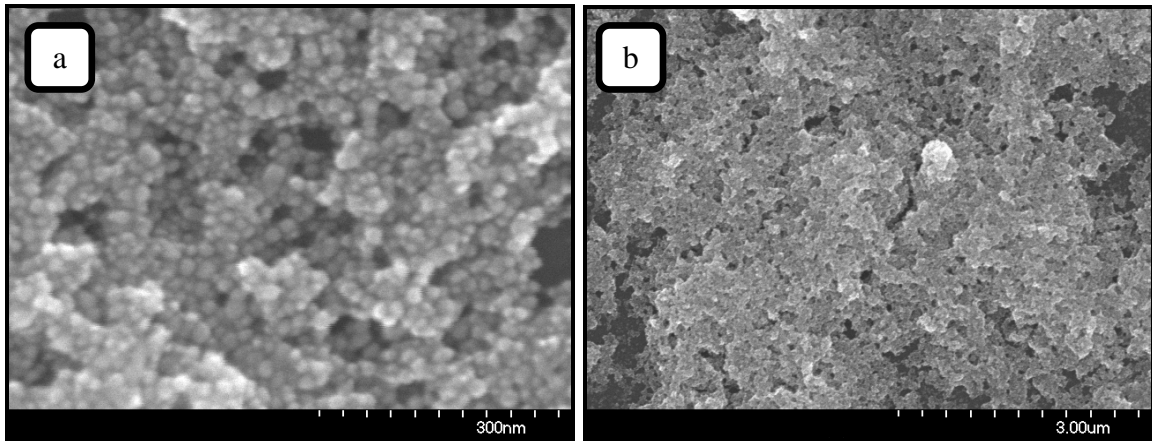
Figure 6.15 SEM images of sintered microstructures, pattern II. Images show the a) bonding of individual nanoparticles and b) layer of nanoparticles

The primary objective of the nanoparticles deposition process was to develop micro-sensing and micro-actuating devices where electrical conductivity is of importance. Unless nanoparticles are bonded through complete melting, the deposited microstructure obtained through sintering would be porous in nature. The effectiveness of sintered depositions to be used as charge carriers can be examined using Percolation Theory. Considering the deposition microstructure as a network between silver nanoparticles, the electrical conductivity can be modeled mathematically as a two dimensional network of particles either bonded (with probability p) or unbounded (with probability 1-p) to adjacent particles. Probability that there exists an electrical path throughout the network in such a case is either 1 or 0, either conductive or nonconductive.

To produce electrically conductive micropatterns, a conductive path or a series of nanoparticles arranged in a definite loop is required. The conductive path between the depositions can be crudely evaluated by drawing a conductive path, i.e. a line across the image connecting particles visibly bonded to each other. Deposition consists of partially complete paths are primarily seen in Figure 6.16 (a) whereas complete path formations are seen in Figure 6.16 (b). The electrical connectivity of microstructures was enhanced by increasing the number of nanoparticles sintered over the substrate surface.

Incomplete conductive paths   Complete conductive paths
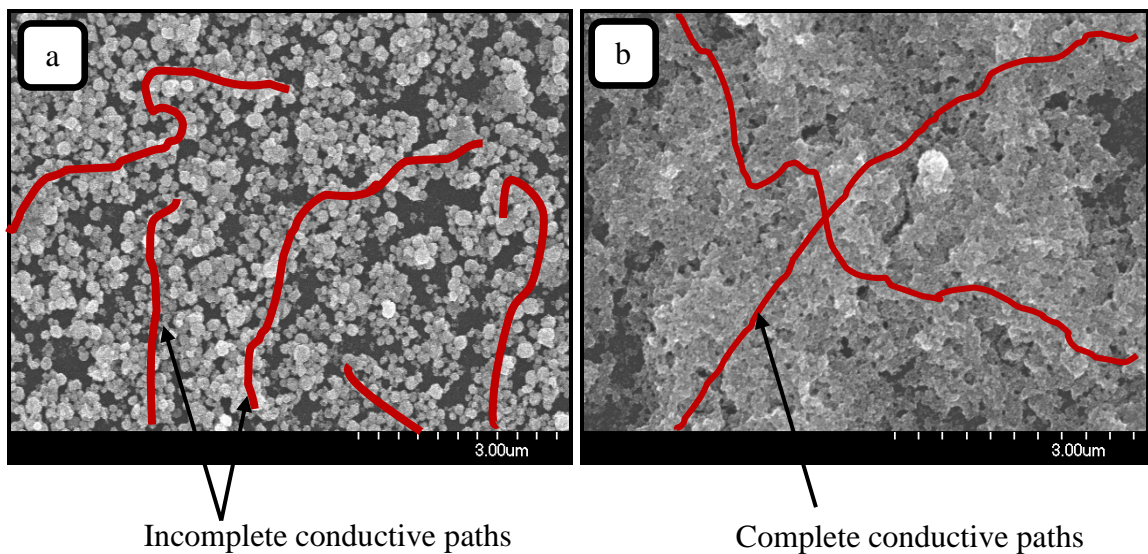
Figure 6.16 Comparison of conductive paths between microstructures. Shown are the microstructures for a) pattern I and b) pattern II. Numerous complete paths exist across (b) whereas partial paths exist across (a)

The sintered depositions and comparison of conductive paths is confined to a small sample of the deposition surface which provides a local perspective of the deposition rather than an overall perspective. Superior microstructures having complete conductive paths throughout the deposit are feasible and can be achieved by further improvements to the process.

7. SUMMARY AND CONCLUSION

In order to develop the microfabrication process, experiments were conducted to identify the parameters and their influences on the working of the microfabrication process. Parameters influence on the deposition of nanoparticles onto the substrate was examined. Flowrate and electric field were found to influence the jet length, spray shape and distribution. A designed experiment was used to identify the parameters that influence the spray and their interactions. The results of the designed experiment showed that the most significant factors were flowrate and cathode distance. Interactions between the independent parameters were not found to be significant. Standoff distance was found to influence the formation of nanoparticle thin films and their size. The use of a slanted tip extractor was useful in having the nanoparticles spray coaxial to the projected laser pattern without using an external device. Corrections due to offsetting either the nanoparticles flow or the laser pattern system if was avoided.

Based on the parameters studied, changes were proposed to the microfabrication system. The electrospray aerosol generator was eliminated from the setup and instead, the principle of electrospraying was used to directly spray and deposit nanoparticles onto the substrate. The need for a carrier gas was also eliminated by removing the aerosol generator but was replaced by a compressed gas line that would be required to flush the deposition chamber clean from contamination of nanoparticles. The coaxial nozzle system was replaced by directly spraying nanoparticles onto the substrate. The deposited nanoparticles were found to be concentrated over a small area on the surface and thus the need for collimating devices such as aerodynamic lenses was eliminated. Using a collimation apparatus would require the nanoparticles transportation system and the laser

pattern system to be offset and a need to correct the misalignment. This was eliminated in the proposed design. Hence the prototype was modified to have improved reliability during deposition while being cheaper to construct and smaller in size.

Finally, the proposed prototype setup was tested to see the functionality of the deposition process to fabricate microstructures. A greater number of nanoparticles were found to have been transported and deposited onto the substrate. Moreover, since depositions were obtained for numerous trials, the process was found to be repeatable. The deposition of nanoparticles onto the substrate was studied to identify the distribution of deposited nanoparticles. This was done using image analysis and constructing 2D surface profiles and 3D surface plots. The dispersion was found to be polydisperse having a Gaussian tail. The dispersion was verified by examining a sintered deposition under an optical microscope and was established to be the same. Roughness of the deposit was also evaluated through image analysis. It was observed that the roughness on the deposition surface increased with prolonging deposition. These results were compared to results obtained using an atomic force microscope and was found that the roughness increased with increasing deposition layers. Silver nanoparticles were deposited onto a silicon substrate using the apparatus and the nanoparticles were sintered using the patterned laser beam. Although initially the sintered depositions were found to form a ball like structure, by changing the duration of deposition and sintering, a continuous layer of microstructures were formed. Though microscopic examinations give a local perspective over a small area, further work would be required to improve the microstructure over the complete microstructure.

8. RECOMMENDATIONS

The results of this investigation revealed a possibility of further improvements to direct write microstructures. The primary initiative should be to illuminate the spray ensuring complete visibility of the spray profile. Using the laser beam, a laser stripe can be generated by passing the laser beam through a glass rod or, replacing the laser beam with an alternate source of illumination (incandescent, LED, UV). With a completely illuminated spray, the designed experiment can be expanded to study the output responses of jet length and core diameter for the input parameters previously used in the experiment. An experiment could be conducted to evaluate the changes in spray geometry to obtain a relationship between flowrate and input current.

Development of an experimental method to find the velocity of the nanoparticles extracted from the electrospray is required. The velocity of the nanoparticles can be evaluated to the theoretical velocity of the particles. Knowledge on the velocity of the nanoparticles can be expanded to predict the probability of nanoparticles rebounding from the substrate surface upon collision. A study on preparation of the nanoparticle ink solution would be beneficial in controlling the spray. Critical properties such as viscosity, surface tension and conductivity of the ink solvent depend upon factors such as the solvent, solute and nanoparticle diameter. These factors are easily variable and their effects on the spray would have to be studied to improve the deposition process further. The emitter geometry has a high influence on the formation of the electric field formation. The mechanism of electric field formation using the slanting emitter can be studied to maximize the process operation and an optimum angle could be identified. The motion of liquid droplets along a thin wire can be controlled using an electric field and

the possibility of using this mechanism could be investigated to transport and deposit nanoparticles.

Lasers beams have been used to transport nanoparticles as in the case of optical tweezers. Similarly, the possibility of using the optical gradient forces of the projected laser beam to carry and deposit nanoparticles onto the substrate can be explored. In order to produce and replicate microstructures of precise dimensions, the process has to be calibrated to attain the desired dimensions. Uniform illumination from the micromirrors can be achieved by calibrating a grayscale image to the input slide used to control the individual mirrors.

BIBLIOGRAPHY

[1] W. Fang, "Direct Microstructure Deposition by Micromirror Direct Patterning and Laser Sintering of Nanaoparticles," Unpublished master's thesis, 2006

[2] N. R. Bieri, J. Chung, S. E. Haferl, D. Poulikakos and C. P. Grigoropoulos, "Microstructuring by Printing and Laser Curing of Nanoparticle Solutions," Applied Physics Letters, 2003

[3] N. R. Bieri, J. Chung, D. Poulikakos and C. P. Grigoropoulos, "Manufacturing of Nanoscale Thickness Gold Lines by Laser Curing of a Discretely Deposited Nanoparticle Suspension," Superlattices and Microstructures, 2003

[4] J. Chung, S Ko, N.R. Bieri, C.P. Grigoropoulos and D. Poulikakos, "Conductor Microstructures by Laser Curing of Printed Gold Nanoparticle Ink," Applied Physics Letters, Vol 84, 2004

[5] E.M. Nadgorny, C. Zhou, J. Drelich and R. Zahn, "MTU Laser-Based Direct-Write Techniques: Recent Developments and Nanoparticles Patterning Results," Proceedings to the Materials Research Society, 2003

[6] J. Xu, J. Drelich and E.M. Nadgorny, "Laser Based Patterning of Gold Nanoparticles into Microstructures," Langmuir, 2004

[7] S.H. Ko, H. Pan, C.P. Grigoropoulos, C.K. Luscombe, J.M.J. Frechet and D. Poulikakos, "All Inkjet Printed Flexible Electronics Fabrication on a Polymer Substrate by Low Temperature High Resolution Selective Laser Sintering of Metal Nanoparticles," Nanotechnology 18, 2007

[8] S B. Fuller, E J. Wilhelm and J M. Jacobson, "Ink-Jet Printed Nanoparticle Microelectromechanical Systems," Journal of Microelectromechanical Systems, Vol 11, 2002

[9] T.Y. Choi and D. Pouloikakos, "Fountain-pen Based Laser Micro Structuring With Gold Nanoparticle Inks," Applied Physics Letters, Volume 85, 2004

[10] Dae-Young Lee, Yun-Soo Shin, Sung-Eun Park, Tae-U Yu and Jungho Hwang, "Electrohydrodynamic Printing of Silver Nanoparticles by Using a Focused nanocolloid jet," Applied Physics Letters, 2007

[11] C. Sun, N. Fang, D. M. Wu and X. Zhang, "Projection Micro-Stereolithography Using Digital Micro-mirror Dynamic Mask," Sensors and Actuators A, 2005

[12] Y. Lu, G. Mapili, G. Suhail, S. Chen and K. Roy, "A digital micro-mirror device-based system for the microfabrication of complex, spatially patterned tissue engineering scaffolds," Wiley InterScience, 2006

[13] A. Bertsch, S. Jiguet and P. Renaud, "Microfabrication of Ceramic Components by Microstereolithography," Journal of Micromechanics and Microengineering, 2004

[14] G. Xu, X. Ma, H. Pan and S. Hu, "Research of Micro-Stereolitigraphy System with Dynamic Pattern Generator," Applied Mechanics and Materials, Vols 16-19, 2009

[15] Chi Zhou, Yong Chen and Richard A. Waltz, "Optimized Mask Image Projection for Solid Freeform Fabrication," Proceedings to the ASME International Design Engineering Technical Conference, 2009

[16] Chi Zhou and Yong Chen, "Additive Manufacturing Based on Multiple Calibrated Projectors and Its Mask Image Planning," Proceedings to the ASME 2010 International Design Engineering Technical Conference, 2010

[17] A. Jaworek and A.T. Sobczyk, "Electrospraying Route to Nanotechnology: An Overview," Journal of Electrostatics, 2007

[18] O.V. Salata, "Tools of Nanotechnology: Electrospray," Current Nanoscience 2005

[19] G. Taylor, "Disintegration of Water Drops in an Electric Field," Proceedings to the Royal Society of London, 1964

[20] O. Wilhelm, L. Mädler and S.E. Pratsinis, "Electrospray Evaporation and Deposition," Journal of Aerosol Science, 2003

[21] A. Jaworek and A. Krupa, "Classification of the Modes of EHD Spraying," Journal of Aerosol Science, Vol 30, 1999

[22] A. Jaworek and A. Krupa, "Jet and Drops Formation in Electrohydrodynamic Spraying of Liquids. A Systematic Approach," Experiments in Fluids, 1999

[23] Hyun-Ha Kim, Atsuchi Ogata and Jong-Ho Kim, "High Speed Camera Observation of Electrospray," Electrostatics Joint Conference, Poster Session, 2009

[24] R. P. A. Hartman, D. J. Brunner, D. M. A Camelot, J.C.M. Marijnissen and B. Scarlett, "Jet Break-Up in Electrohydrodynamic Atomization in the Cone-Jet Mode," Journal of Aerosol Science, Vol 31, 2000

[25] A. Jaworek, A. Krupa, A. T. Sobczyk, M. Lackowski, T. Chech, S. Ramakrishna, S. Sundarrajan and D. Pliszka, "Electrospray Nanocoating of Microfibres," Solid State Phenomena Vol. 140, 2008

[26] Ivo B. Rietveld, Kei Kobayashi, Hirofumi Yamada and Kazumi Matsushige, "Electrospray Deposition, Model, and Experiment: Towards General Control of Film Morphology," Journal of Physical Chemistry B, 2006

[27] C.N. Ryan, K.L. Smith, M.S. Alexander and J.P.W Stark, "Effect of Emitter Geometry on Flowrate Sensitivity to Voltage in Cone-jet Mode Electrospray," Journal of Applied Physics, 2009

[28] K.L. Smith, M.A. Alexander and J.P.W. Stark, "The Sensitivity of Volumetric Flowrate to Applied Voltage in Cone-jet Mode Electrospray and the Influence of Solution Properties and Emitter Geometry," Physics of Fluids 18, 2006

[29] Xiaopeng Chen, Laibing Jia, Xiezhen Yin, Jiusheng Cheng and Jian Lu, "Spraying Modes in Coaxial Jet Electrospray with Outer Driving Liquid," Physics of Fluids, 2005

[30] Alfonso M. Ganan-calvo, Jose M. Lopez-herrera and Pascual Riesco-chueca, "The combination of Electrospray and flow focusing," Journal of Fluid Mechanics, 2006

[31] Xiaoliang Wang, Frank Einar Kruis and Peter H. McMurphy, "Aerodynamic Focusing of Large Particles: 1. Guidelines for Designing Lenses for Nanoparticles," Aerosol Science and Technology, 2005

[32] Xiaoliang Wang and Peter H. McMurry, "A Design Tool for Aerodynamic Lens Systems," Aerosol Science and Technology, 2006

[33] J.E. Brockmann, R.C. Dykhuizen, R. Cote and T. Roemer, "Aerodynamic Focusing of Large Particles," Proceedings to the 5th International Aerosol Conference, 1998

[34] Kwang-Sung Lee, Sung-Woo Cho and Donggeun Lee, "Development and Experimental Evaluation of Aerodynamic Lens as an Aerosol Inlet of Single Particle Mass Spectrometry," Journal of Aerosol Science, 2007

[35] Jin-Won Lee, Min-Young Yi and Sang-Min Lee, "Inertial Focusing of Particles with an Aerodynamic Lens in the Atmospheric Pressure Range," Journal of Aerosol Science, 2002

[36] J. Passig, K. Meiwes-Broer and J. Tiggesbāumker, "Collimation of Metal Nanoparticle Beams Using Aerodynamic Lenses," Review of Scientific Instruments, 2006

[37] W.G. Shin, G.W. Mulholland, S.C. Kim and D.Y.H Pui, "Experimental Study of Filtration Efficiency of Nanoparticles Below 20nm at Elevated Temperatures," Journal of Aerosol Sciences, 2008

[38] H. Wang and G. Kasper, "Filtration Efficiency of Nanometer-size Aerosol Particles," Journal of Aerosol Science, 1990

[39] Shintaro Sato, Da-Ren Chen, David Y. H. Pui, "Molecular Dynamics Study of Nanoparticles Collision With a Surface Implication to Nanoparticle Filtration," Aerosol and Air Quality Research, Vol 7, 2007

[40] H. Ichitsubo, T. Hashimoto, M. Alonso and Y. Kousaka, "Penetration of Ultrafine Particles and Ions Clusters Through Wire Screens," Aerosol Science and Technology 24, 1996

[41] M Hasegawa, K Hoshino and M Watabe, "A Theory of Melting in Metallic Small Particles," Journal of Physics F: Metal Physics, 1979

[42] T. Castro, R. Reifenberger, E. Choi and R. P. Andrews, "Size-Dependent Melting Temperature of Individual Nanometer-Sized Metallic Clusters," The American Physical Society, 1990

[43] Sanjeev K. Gupta, Mina Talati and Prafulla K. Jha, "Shape and Size Dependent Melting Point Temperature of Nanoparticles," Materials Science Forum, 2008

[44] Ph. Buffat and J-P. Borel, "Size Effects on the Melting Temperature of Gold Particles," Physical Review A, Vol 13, 1976

[45] T. Bachels, H. Güntherodt and R. Schäfer, "Melting of Isolated Tin Nanoparticles," Physical Review Letters, 2000

[46] W. Luo, W. Hu and S. Xiao, "Size Effect on the Thermodynamic Properties of Silver Nanoparticles," J. Phys. Chem. C 2008

[47] Y. Yasuda, E. Ide and T. Morita, "Low-Temperature Bonding Using Silver Nanoparticles Stabilized by Short-Chain Alkylamines," Japanesse Journal of Applied Physics, 2009

[48] Kyoung-Sik Moon, Hai Dong, Radenka Maric, Suresh Pothukuchi, Andrew Hunt, Yi Li and C. P. Wong, "Thermal Behaviour of Silver Nanoparticles for Low-Temperature Interconnect Applications," Journal of Electronic Materials, 2005

[49] P. V. Asharani, Yi Lian Wu, Zhiyuan Gong and Suresh Valiyaveettil, "Toxicity of Silver Nanoparticles in Zebrafish Models," Nanotechnology, 2008

[50] Jin-Sook Hyun, Byoung Seok Lee, Hyeon Yeol Ryu, Jae Hyuck Sung, Kyu Hyuck Chung and Il Je Yu, "Effects of repeated silver nanoparticles exposure on the histological structure and mucins of nasal respiratory mucosa in rats," Toxicology Letters, 2008

VITA

Vivekram Ramanathan, son of Thiruveni Ramanathan and Ramanathan Arunasalam was born on September 17, 1984 in Chennai, India. He received his B. Tech in Mechanical Engineering from SRM University, Chennai, India in July 2007. Vivek then began pursuing his master's degree in Manufacturing Engineering at Missouri University of Science and Technology, Rolla, USA under the guidance of Dr. Frank W. Liou, Professor of Mechanical Engineering.

During his graduate degree, Vivek worked as a Graduate Research Assistant in the Laser Aided Manufacturing Processes Laboratory (LAMP) at Missouri S&T. His research was focused on developing a new process to produce micro components by laser sintering. Vivek got his Masters in Manufacturing Engineering in July 2010. He also obtained his Graduate Certificate in Lean Six Sigma from Missouri S&T in May 2010.

Vivek is a member of the American Society of Mechanical Engineering (ASME) and the Society of Manufacturing Engineers (SME). He actively served in the SME Executive Committee in 2008.